Research Paper

GEOSPHERE

GEOSPHERE, v. 16, no. 5

https://doi.org/10.1130/GES02240.1

12 figures (2 are interactive); 3 tables;
1 supplemental file

CORRESPONDENCE: jeff@geology.cwu.edu

CITATION: Lee, J., Hoxey, A.K.R., Calvert, A., and Dubyoski, P., 2020, Plate boundary trench retreat and dextral shear drive intracontinental fault-slip histories: Neogene dextral faulting across the Gabbs Valley and Gillis Ranges, Central Walker Lane, Nevada: Geosphere, v. 16, no. 5, p. 1249–1275, https://doi.org/10.1130/GES02240.1.

Science Editor: Andrea Hampel
Associate Editor: Andrew V. Zuza

Received 4 February 2020
Revision received 9 April 2020
Accepted 17 June 2020

Published online 31 July 2020

GOLD OPEN ACCESS

THE GEOLOGICAL SOCIETY OF AMERICA®

This paper is published under the terms of the CC-BY-NC license.

© 2020 The Authors

Plate boundary trench retreat and dextral shear drive intracontinental fault-slip histories: Neogene dextral faulting across the Gabbs Valley and Gillis Ranges, Central Walker Lane, Nevada

Jeffrey Lee[1,2], Andrew K.R. Hoxey[1,*], Andrew Calvert[3], and Peter Dubyoski[1,†]

[1]Department of Geological Sciences, Central Washington University, Ellensburg, Washington 98926, USA
[2]Department of Geophysics, Colorado School of Mines, Golden, Colorado 80401, USA
[3]Volcano Science Center, U.S. Geological Survey, 345 Middlefield Road, MS 910, Menlo Park, California 94025, USA

ABSTRACT

The spatial-temporal evolution of intracontinental faults and the forces that drive their style, orientation, and timing are central to understanding tectonic processes. Intracontinental NW-striking dextral faults in the Gabbs Valley–Gillis Ranges (hereafter referred to as the GVGR), Nevada, define a structural domain known as the eastern Central Walker Lane located east of the western margin of the North American plate. To consider how changes in boundary type along the western margin of the North American plate influenced both the initiation and continued dextral fault slip to the present day in the GVGR, we combine our new detailed geologic mapping, structural studies, and $^{40}Ar/^{39}Ar$ geochronology with published geologic maps to calculate early to middle Miocene dextral fault-slip rates. In the GVGR, Mesozoic basement is nonconformably overlain by a late Oligocene to Miocene sequence dominated by tuffs, lavas, and sedimentary rocks. These rocks are cut and offset by four primary NW-striking dextral faults, from east to west the Petrified Spring, Benton Spring, Gumdrop Hills, and Agai Pah Hills–Indian Head faults. A range of geologic markers, including tuff- and lava-filled paleovalleys, the southern extent of lava flows, and a normal fault, show average dextral offset magnitudes of 9.6 ± 1.1 km, 7.0 ± 1.7 km, 9.7 ± 1.0 km, and 4.9 ± 1.1 km across the four faults, respectively. Cumulative dextral offset across the GVGR is 31.2 ± 2.3 km. Initiation of slip along the Petrified Spring fault is tightly bracketed between 15.99 ± 0.05 Ma and 15.71 ± 0.03 Ma, whereas slip along the other faults initiated after 24.30 ± 0.05 Ma to 20.14 ± 0.26 Ma. Assuming that slip along all four faults initiated at the same time as the Petrified Spring fault yields calculated dextral fault-slip rates of 0.4 ± 0.1–0.6 ± 0.1 mm/yr, 0.4 ± 0.1–0.5 ± 0.1 mm/yr, 0.6 ± 0.1 mm/yr, and 0.3 ± 0.1 mm/yr on the four faults, respectively. Middle Miocene initiation of dextral fault slip across the GVGR overlaps with the onset of normal slip along range-bounding faults in the western Basin and Range to the north and the northern Eastern California shear zone to the south. Based on this spatial-temporal relationship, we propose that dextral fault slip across the GVGR defines a kinematic link or accommodation zone between the two regions of extension. At the time of initiation of dextral slip across the GVGR, the plate-boundary setting to the west was characterized by subduction of the Farallon plate beneath the North American plate. To account for the middle Miocene onset of extension across the Basin and Range and dextral slip in the GVGR, we hypothesize that middle Miocene trench retreat drove westward motion of the Sierra Nevada and behind it, crustal extension across the Basin and Range and NW-dextral shear within the GVGR. During the Pliocene, the plate boundary to the west changed to NW-dextral shear between the Pacific and North American plates, which drove continued dextral slip along the same faults within the GVGR because they were fortuitously aligned subparallel to plate boundary motion.

INTRODUCTION

Several fundamental questions in tectonics center on the spatial-temporal evolution of intracontinental faults. Is intraplate strain localized along a few discrete faults or is strain accommodated across a wide zone of faulting and deformation? Is intraplate strain episodic and local or non-episodic and broadly distributed? What controls whether deformation becomes localized into a narrow zone or develops across a wide zone? Does fault slip maintain a constant rate over thousands to millions of years? What forces drive the style, orientation, and timing of intracontinental faulting?

Deformation across the Walker Lane–northern Eastern California shear zone (western U.S. Cordillera) (Fig. 1), a diffuse zone dominated by strike-slip faults superimposed on normal faults, appears to be largely driven by two primary forces: edge forces, a consequence of the relative motion between the Pacific and North American plates, and internal forces (gravitational potential energy), a consequence of variations in plate density structure (e.g., Flesch et al., 2000; Jones et al., 2004; Humphreys and Coblentz, 2007). Since the Pacific plate came in contact with the North American plate at ca. 28 Ma, transform slip has been the dominant plate interaction along much of the western margin of the United States (Atwater and Stock, 1998). Atwater and Stock's (1998) benchmark reconstructions of motion of the Pacific plate relative to the North America plate, built on data resolution at 3–9 Ma intervals, show that the rate

*Now at Department of Geology, University of Kansas, Lawrence, Kansas 66045, USA
†Now at 4411 Ridge Avenue, Halethorpe, Maryland 21227, USA

Downloaded from http://pubs.geoscienceworld.org/gsa/geosphere/article-pdf/16/5/1249/5148564/1249.pdf
by University of Nevada Reno user

of relative plate motion substantially increased between ca. 12–8 Ma, slowed down until ca. 5 Ma, and then increased to the present day. The direction of plate motions remained constant until ca. 8 Ma, at which time the direction rotated to a more northerly azimuth indicating a greater degree of transform slip that has continued to the present day.

More recent reconstructions of Pacific–North America plate rotations since ca. 20 Ma provide greater temporal resolution (~1 m.y. intervals), which offers new insights into the rate and rotation of the Pacific plate relative to North America plate (DeMets and Merkouriev, 2016). In these reconstructions, the rate of Pacific plate motion relative to the North America plate increased by ~70% between 19.7 to ca. 9 Ma but changed little (~2%) since 8 Ma and changed less than ~2% during the past ~4 m.y. (DeMets and Merkouriev, 2016). The slip direction between the two plates shows progressive clockwise rotation of ~25° during most of the past ~20 m.y., except for a possible hiatus between 9 and 5 Ma, imparting an increasing component of transform slip along the plate boundary with time (DeMets and Merkouriev, 2016).

In the Atwater and Stock (1998) reconstructions, the relatively abrupt increase in rate and change to a more transform-like plate boundary at ca. 8 Ma, and, therefore, less extensional plate boundary deformation, implies that the dextral shear deformation rates in the western U.S. Cordillera, including the Walker Lane, should increase and extension rates should slow. In contrast, in the DeMets and Merkouriev (2016) reconstructions, the nearly constant increase in plate rate and plate boundary transform slip component implies a relatively constant increase in dextral shear deformation along the western margin of the U.S. Cordillera.

In addition to changes in Pacific–North America plate boundary motion rates and slip direction, a change in the gravitational potential energy is postulated in the region of the southern Sierra Nevada. Uplift of the southern Sierra Nevada range accelerated during the Pliocene–Quaternary (e.g., Jones, 1987; Wakabayashi and Sawyer, 2001; Jones et al., 2004; Stock et al., 2004, 2005). This pulse of uplift is postulated to be the consequence of removal of mantle lithosphere (e.g., Jones et al., 2004; Saleeby et al., 2012; and references therein), and is hypothesized to drive a local increase in gravitational potential energy (e.g., Jones et al., 2004). The increase in gravitational potential energy should increase strain rates during the Pliocene within an ~50 km area east of the Sierra Nevada, including the western Basin and Range, Mina deflection, and northern Eastern California shear zone, and perhaps the Central Walker Lane (Jones et al., 2004) (Figs. 1 and 2). Geologic data in support of this hypothesis include Pliocene initiation of fault slip or renewed fault slip documented along the eastern Inyo fault zone and the Hunter Mountain fault (Lee et al., 2009), the Queen Valley fault (Stockli et al., 2003), the southwestern Mina deflection (Nagorsen-Rinke et al., 2013; DeLano et al., 2019), all in relatively close proximity to the southern Sierra Nevada, and in the Central Walker Lane along the Wassuk Range front normal fault (Stockli et al., 2002) (Fig. 2).

In the eastern part of the Central Walker Lane, Nevada, in the Gabbs Valley–Gillis Ranges (hereafter referred to as the GVGR region), located east of the Wassuk Range (Figs. 2 and 3), dextral faulting has been proposed to initiate

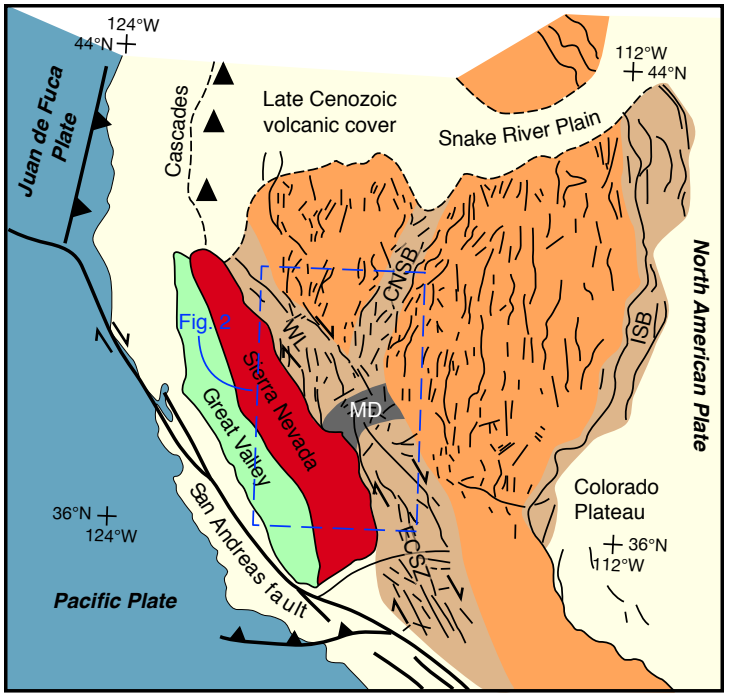

Figure 1. A. Simplified tectonic map of the western U.S. Cordillera showing the modern plate boundaries and tectonic provinces. Basin and Range Province is in light brown, superimposed upon which are the Central Nevada seismic belt (CNSB), eastern California shear zone (ECSZ), Intermountain seismic belt (ISB), and Walker Lane (WL) in tan; Mina deflection (MD) is in dark gray. Blue rectangle marks the location of Figure 2.

as early as ca. 25 Ma (Ekren et al., 1980; Ekren and Byers, 1984), to as late as ca. 10 Ma (Hardyman and Oldow, 1991). The magnitude, timing, and rate of dextral fault slip is not well characterized across the GVGR; therefore, this region is an excellent location for assessing the long-term (10^6 yr) evolution of a system of intracontinental dextral faults, and for testing whether there is a temporal, and therefore causal, relationship between changes in the timing of dextral fault slip and changes in timing of the driving forces in the western U.S. Cordillera.

To address these issues, herein we combine new results from our detailed geologic mapping at 1:12,000 scale, structural studies, and $^{40}Ar/^{39}Ar$ geochronology on volcanic rocks with published geologic maps and geochronology to characterize the spatial-temporal distribution of fault slip along four major and two minor NW-striking dextral faults, distributed over ~1650 km^2 across the GVGR (Figs. 2 and 3). Our field studies document several volcanic-filled paleovalleys, which, along with other geologic markers, we use to measure the magnitude of dextral offset across these faults and to calculate fault-slip

Downloaded from http://pubs.geoscienceworld.org/gsa/geosphere/article-pdf/16/5/1249/5148564/1249.pdf
by University of Nevada Reno user

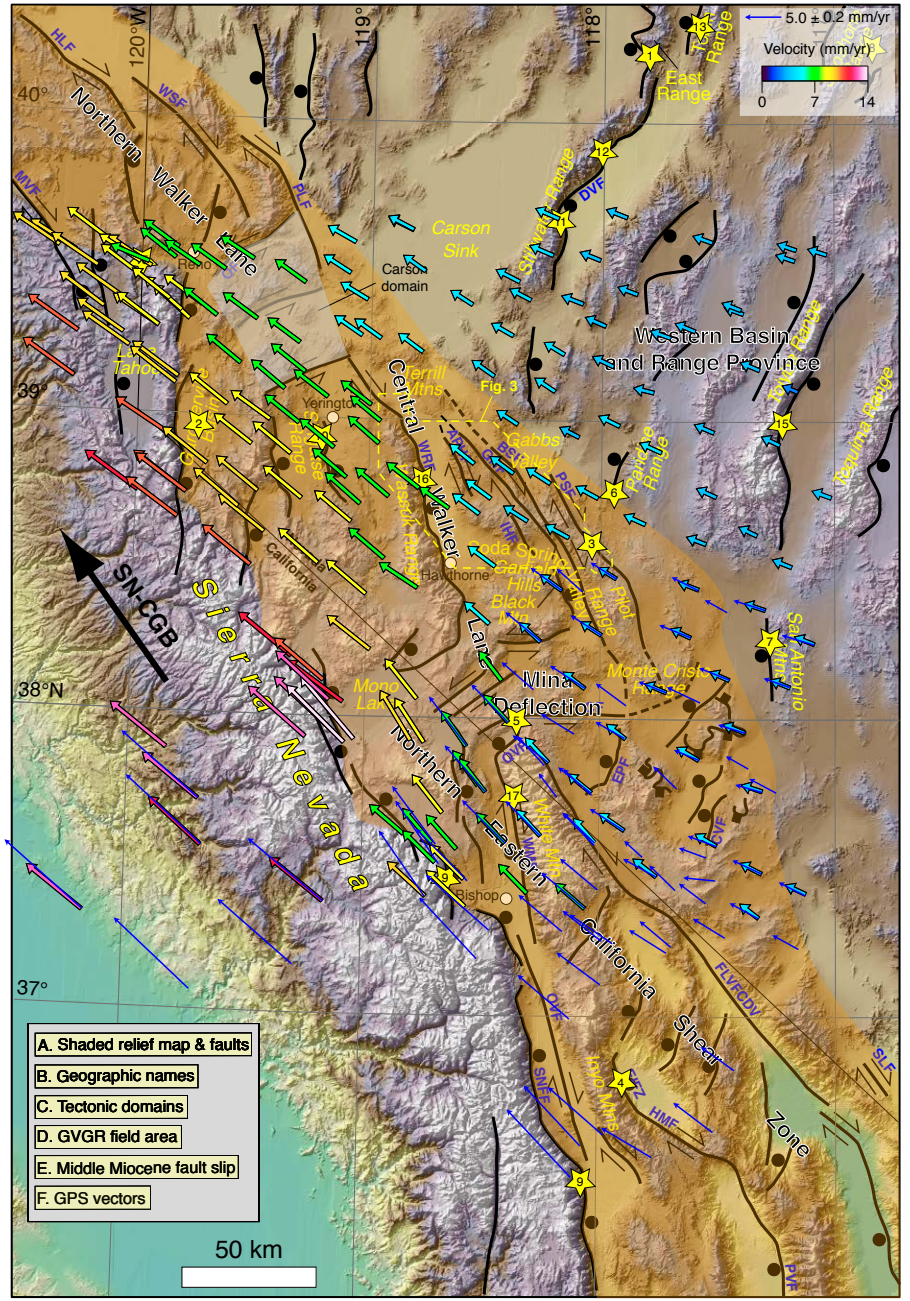

Figure 2. Layer A. Shaded relief map showing major Quaternary faults in central Walker Lane, Mina deflection, northern Eastern California shear zone, and western Basin and Range Province. Heavy black arrow shows the present-day azimuth of motion of the Sierra Nevada block with respect to the central Great Basin (SN-CBG) (Bennett et al., 2003). Fault abbreviations: APHF—Agai Pah Hills fault; BSF—Benton Spring fault; CF—Coaldale fault; CVF—Clayton Valley fault; EIFZ—Eastern Inyo fault zone; EPF—Emigrant Peak fault; FLVFCDV—Fish Lake Valley–Furnace Creek–Death Valley fault zone; GHF—Gumdrop Hills fault; HLF—Honey Lake fault; HMF—Hunter Mountain fault; IHF—Indian Head fault; MVF—Mohawk Valley fault; OF—Olinghouse fault; OVF—Owens Valley fault; PLF—Pyramid Lake fault; PSF—Petrified Spring fault; PVF—Panamint Valley fault; QVF—Queen Valley fault; SLF—Stateline fault; SNFF—Sierra Nevada frontal fault zone; WMF—White Mountains fault zone; WRF—Wassuk Range fault; WSF—Warm Springs fault. Layer B. Geographic names. Layer C. Tectonic domains. Semi-transparent brown shows the Walker Lane–northern Eastern California shear zone. Layer D. Yellow dashed polygon shows the location of the Gabbs Valley–Gillis Ranges (GVGR) field area (see Fig. 3). Layer E. Yellow stars show the locations of documented middle Miocene fault-slip initiation age. Numbers in the stars are tied to numbers in Table 3. Layer F. Thin blue arrows show GPS velocities relative to stable North America (ITRFNA2005 reference frame) from Lifton et al. (2013), and heavy multi-colored arrows show GPS velocities relative to stable North America (NA12 North America reference frame) from Bormann et al. (2016). GPS velocity scales are in the upper right corner of the map. Maps, labels, and data sets for this figure are organized in a series of layers that may be viewed separately or in combination using the capabilities of the Acrobat (PDF) layering function (click "Layers" icon along vertical bar on left side of window for display of available layers; turn layers on or off by clicking the box that encompasses the layer label located within the gray box in the lower left corner of the map). If reading the full-text version of this paper, view the layers of the figure by downloading the PDF or view the figure here: https://doi.org/10.1130/GEOS.S.12498458.

Figure 2 is interactive. If reading the full-text version of this paper, view the layers of the figure by downloading the PDF or view the figure here: https://doi.org/10.1130/GEOS.S.12498458.

Downloaded from http://pubs.geoscienceworld.org/gsa/geosphere/article-pdf/16/5/1249/5148564/1249.pdf
by University of Nevada Reno user

Figure 3 is interactive and is intended to be viewed at a width of 64 cm. To view the layers of Figure 3 if reading the full-text version of this paper or to view the figure at the suggested size, please visit https://doi.org/10.1130/GEOS.S.12500744.

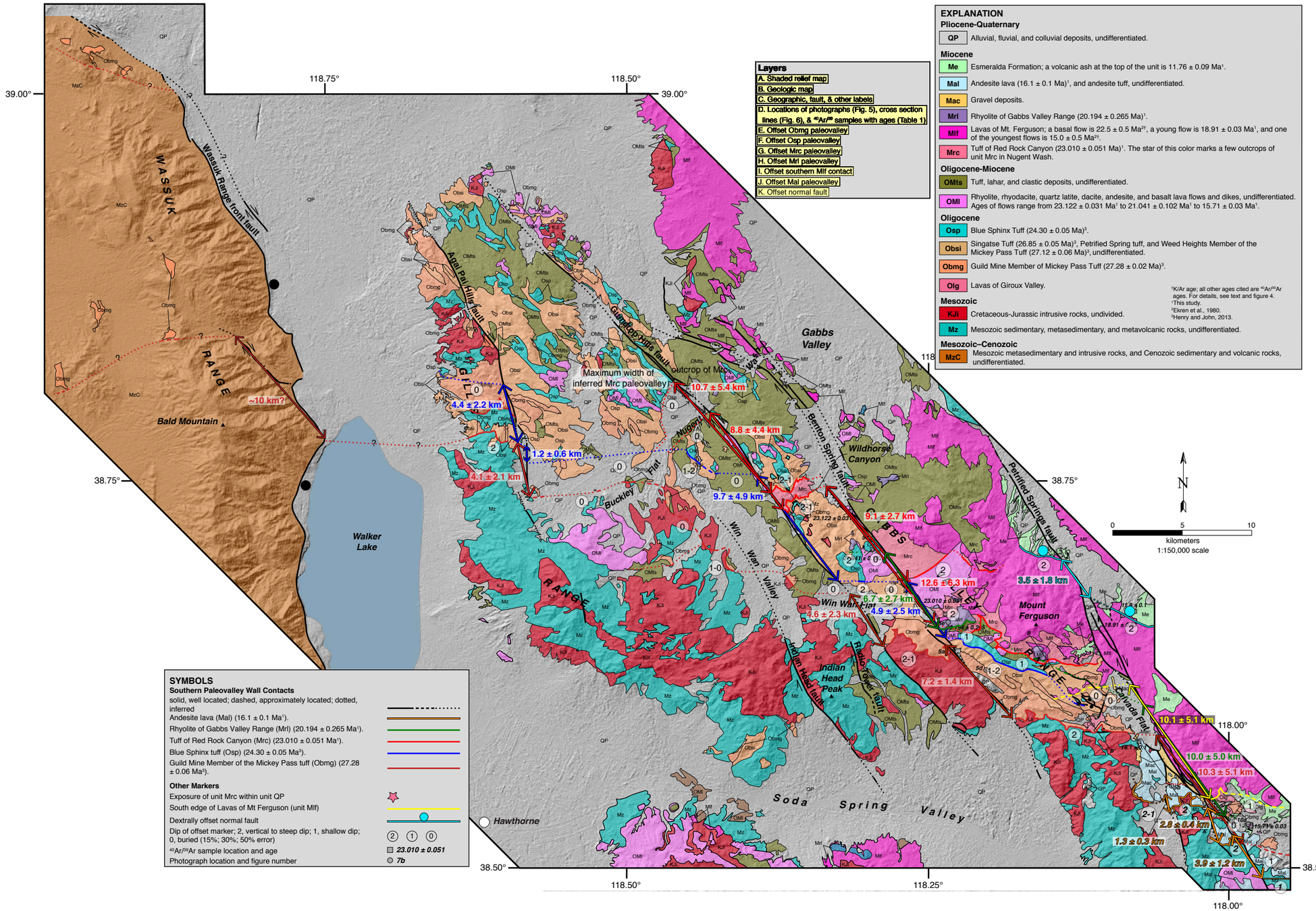

Figure 3. Layer A. Shaded relief map of the Gabbs Valley, Gillis, and Wassuk ranges, Nevada. Layer B. Simplified geologic map of the Gabbs Valley, Gillis, and Wassuk ranges. Sources of geologic mapping: Bingler (1978); Hardyman (1980); Stewart et al. (1981); Ekren and Byers (1985a, 1985b, 1986a, 1986b); Dilles (1992); Hoxey et al. (2020); this study. Layer C. Geographic names for major mountains, valleys, canyons, flats, washes, and lakes; fault names, and other labels. Layer D. Locations of photographs (see Fig. 5), cross-section lines (see Fig. 6), and $^{40}Ar/^{39}Ar$ sample locations with ages (see Table 1). Layers E–J. Southern paleovalley wall contacts and measured dextral offsets for paleovalley infilling units Obmg, Osp, Mrc, Mrl, and Mal, respectively. Layer I. Southern contact of unit Mlf and measured dextral offset. Layer K. Intersection line defined by normal fault–hanging-wall contact between units Mlf and Me and measured dextral offset. Maps, labels, and data sets are organized in a series of layers that may be viewed separately or in combination using the capabilities of the Acrobat (PDF) layering function (click "Layers" icon along vertical bar on left side of window for display of available layers; turn layers on or off by clicking the box that encompasses the layer label located within the gray box in the upper right part of the figure). Figure 3 is intended to be viewed at a width of 64 cm. To view the layers of Figure 3 if reading the full-text version of this paper or to view the figure at the suggested size, please visit https://doi.org/10.1130/GEOS.S.12500744.

Downloaded from http://pubs.geoscienceworld.org/gsa/geosphere/article-pdf/16/5/1249/5148564/1249.pdf
by University of Nevada Reno user

histories at time scales of 10^6 years. To evaluate the forces that drove the style, orientation, and timing of dextral faulting in the Central Walker Lane, we compare the temporal relation between our documented timing and rates of fault slip to the proposed timing of changes in rates and direction of plate boundary slip and timing of changes in gravitational potential energy.

TECTONIC AND GEOLOGICAL SETTING OF THE CENTRAL WALKER LANE

Geologic, geodetic, and plate reconstruction studies indicate the Pacific plate moves northwest at ~50 mm/yr relative to the stable North American continent (e.g., Dokka and Travis, 1990; Dixon et al., 1995; Bennett et al., 2003; DeMets and Merkouriev, 2016) (Fig. 1). Approximately 20%–25% of Pacific–North American plate boundary shear is partitioned into the Eastern California Shear Zone–Walker Lane, an ~25–130-km-wide zone of dextral shear extending from the Mojave Desert northward, along the eastern flank of the Sierra Nevada and across the western boundary of the Basin and Range Province, into western Nevada and northeastern California (e.g., Stewart, 1988; Dokka and Travis, 1990; Dixon et al., 1995; Bennett et al., 2003; Faulds and Henry, 2008) (Figs. 1 and 2).

The Central Walker Lane is an ~130-km-wide dextral shear zone flanked by the Sierra Nevada to the west and Basin and Range extensional faults to the east (e.g., Faulds and Henry, 2008; Bormann et al., 2016) (Fig. 2). The ~45-km-wide eastern Central Walker Lane, located across the GVGR (north and east of Hawthorne, Nevada) is flanked by the Wassuk Range to the west and Western Basin and Range extensional faults to the east (see dashed yellow polygon in Fig. 2). The GVGR is underlain by strongly deformed Mesozoic sedimentary and intrusive rocks nonconformably overlain by Cenozoic volcanic and sedimentary rocks truncated and offset by NW-SE striking dextral faults that define the structural fabric (Hardyman, 1980; Ekren et al., 1980; Ekren and Byers, 1985a, 1985b, 1986a, 1986b; Stewart et al., 1981; Hoxey et al., 2020; this study) (Figs. 2 and 3). The major dextral faults exposed in the GVGR can be divided into two groups based on relative length (Fig. 3): (1) from east to west, the four major dextral faults (fault lengths of ~25–55 km) are the Petrified Spring, Benton Spring, Gumdrop Hills, and Agai Pah Hills faults and (2) from east to west, the two minor faults (fault lengths of ~6–12 km), the Radio Tower and Indian Head faults (Hardyman, 1980; Stewart, 1988; Hardyman and Oldow, 1991; Ekren and Byers, 1985a, 1985b, 1986a, 1986b; Hoxey et al., 2020; this study).

Using geologic map data and K-Ar geochronology on volcanic rocks, earlier workers inferred that dextral fault slip across the GVGR may have initiated as early as ca. 25 Ma (Ekren et al., 1980; Ekren and Byers Jr., 1984), or as late as ca. 10 Ma (Hardyman and Oldow, 1991). Cumulative dextral displacement across five of the dextral faults in the GVGR has been estimated at as little as 26 km to as much as 60 km (Ekren et al., 1980; Ekren and Byers, 1984; Hardyman and Oldow, 1991; Oldow, 1992; Hardyman et al., 2000). The four major, and one minor (Indian Head fault), dextral faults expose fault scarps developed in late Pleistocene to Holocene alluvial surfaces indicating they are still active (e.g., Bell et al., 1999; Wesnousky, 2005; Langille et al., 2016, 2018; Angster, et al., 2019; this study). Low topographic relief in the GVGR compared to the surrounding ranges suggests little normal slip along these faults (Figs. 2 and 3). An elastic block model of GPS velocities yields present-day dextral shear rates parallel to 323°—the present-day azimuth of motion of the Sierra Nevada block relative to the Central Great Basin (SN-CGB) (Bennett et al., 2003)—of 2.7 ± 0.7 mm/yr across the GVGR (Bormann et al., 2016) (Fig. 2).

GEOLOGIC ROCK UNITS AND AGES

Our geologic mapping and structural studies along the Petrified Spring fault, the southern ~60% of the Benton Spring fault, the middle ~33% of the Gumdrop Hills fault, and the Radio Tower and Indian Head faults, combined with geologic mapping by Ekren and Byers (1985a, 1985b, 1986a, 1986b), Stewart et al. (1981), Hardyman (1980), and Hoxey et al. (2020), across the GVGR documents Mesozoic basement units overlain by Oligocene, Miocene, and Pliocene volcanic and sedimentary units, and Quaternary sedimentary units (Figs. 3 and 4). The Mesozoic basement includes intruded sedimentary, metasedimentary, and metavolcanic rocks overlain nonconformably by Oligocene and Miocene volcanic and sedimentary rocks. Pliocene volcanic and sedimentary rocks lie in angular unconformable contact above the Oligocene and Miocene sequence and are in turn overlain unconformably by Quaternary alluvium and colluvium deposits.

Below we briefly describe the map units shown in the geologic map of Figure 3, which covers the GVGR. For simplicity, some of the map units are composed of two or more units mapped at smaller scales by Ekren and Byers (1985a, 1985b, 1986a, 1986b), Hardyman (1980), Stewart et al. (1981), Ekren et al. (1980), and Hoxey et al. (2020), where more detailed descriptions of these units can be found. Detailed map unit descriptions are provided in Figure 4, new and published $^{40}Ar/^{39}Ar$ ages are summarized in Table 1, and a description of $^{40}Ar/^{39}Ar$ analytical techniques, analytical results, age spectra, and probability density plots of ages are provided in the Supplemental File[1].

The oldest rock unit, Mesozoic basement (Mz), is composed of Triassic and Jurassic sedimentary, metasedimentary, and metavolcanic rocks intruded by Jurassic to Cretaceous diorite, granodiorite, quartz monzonite, and granite (KJi) (Figs. 3 and 4).

Lying nonconformably above the Mesozoic basement is a succession of Oligocene and Miocene volcanic and sedimentary rocks (Figs. 3 and 4). Where the unconformity is exposed on the Mesozoic granitoids, we observe up to a several-meters-thick gravel and paleosol sequence defined by subrounded to rounded pebbles, cobbles, and boulders of the bedrock and/or a red weathering horizon composed of grus and corestones on top of strongly fractured bedrock, respectively (Figs. 5A and 5B). At this contact along the northwestern flank of the Gillis Range, root casts, petrified wood, and stream conglomerate were also observed (Eckberg et al., 2005).

Locally exposed on top of this unconformity are basalt Lavas of Giroux Valley (Olg) (Figs. 3 and 4). The Benton Spring Group, a series of rhyolitic to

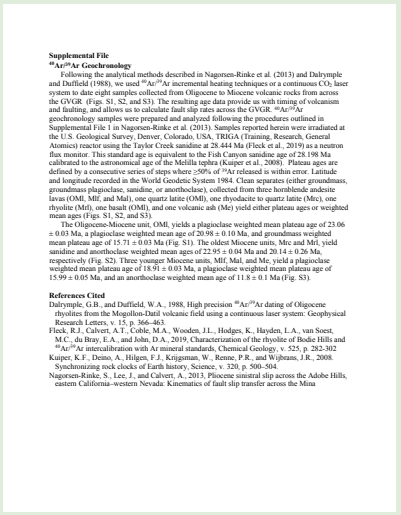

Supplemental File

$^{40}Ar/^{39}Ar$ Geochronology

Following the analytical methods described in Nagorsen-Rinke et al. (2013) and Dalrymple and Duffield (1988), we used $^{40}Ar/^{39}Ar$ incremental heating techniques or a continuous CO_2 laser system to date eight samples collected from Oligocene to Miocene volcanic rocks from across the GVGR (Figs. S1, S2, and S3). The resulting age data provide us with timing of volcanism and faulting, and allows us to calculate fault slip rates across the GVGR. $^{40}Ar/^{39}Ar$ geochronology samples were prepared and analyzed following the procedures outlined in Supplemental File 1 in Nagorsen-Rinke et al. (2013). Samples reported herein were irradiated at the U.S. Geological Survey, Denver, Colorado, USA, TRIGA (Training, Research, General Atomics) reactor using the Taylor Creek sanidine at 28.444 Ma (Fleck et al., 2019) as a neutron flux monitor. This standard age is equivalent to the Fish Canyon sanidine age of 28.198 Ma calibrated to the astronomical age of the Melilla tephra (Kuiper et al., 2008). Plateau ages are defined by a consecutive series of steps where ≥50% of ^{39}Ar released is within error. Latitude and longitude recorded in the World Geodetic System 1984. Clean separates (either groundmass, groundmass plagioclase, sanidine, or anorthoclase), collected from three hornblende andesite lavas (OMl, Mlf, and Mal), one quartz latite (OMl), one rhyodacite to quartz latite (Mrc), one rhyolite (Mrl), one basalt (OMl), and one volcanic ash (Me) yield either plateau ages or weighted mean ages (Figs. S1, S2, and S3).

The Oligocene-Miocene unit, OMl, yields a plagioclase weighted mean plateau age of 23.06 ± 0.03 Ma, a plagioclase weighted mean age of 20.98 ± 0.10 Ma, and groundmass weighted mean plateau age of 15.71 ± 0.03 Ma (Fig. S1). The oldest Miocene units, Mrc and Mrl, yield sanidine and anorthoclase weighted mean ages of 22.95 ± 0.04 Ma and 20.14 ± 0.26 Ma, respectively (Fig. S2). Three younger Miocene units, Mlf, Mal, and Me, yield a plagioclase weighted mean plateau age of 18.91 ± 0.03 Ma, a plagioclase weighted mean plateau age of 15.99 ± 0.05 Ma, and an anorthoclase weighted mean age of 11.8 ± 0.1 Ma (Fig. S3).

References Cited

Dalrymple, G.B., and Duffield, W.A., 1988, High precision $^{40}Ar/^{39}Ar$ dating of Oligocene rhyolites from the Mogollon-Datil volcanic field using a continuous laser system: Geophysical Research Letters, v. 15, p. 366–463.
Fleck, R.J., Calvert, A.T., Coble, M.A., Wooden, J.L., Hodges, K., Hayden, L.A., van Soest, M.C., du Bray, E.A., and John, D.A., 2019, Characterization of the rhyolite of Bodie Hills and $^{40}Ar/^{39}Ar$ intercalibration with Ar mineral standards, Chemical Geology, v. 525, p. 282–302
Kuiper, K.F., Deino, A., Hilgen, F.J., Krijgsman, W., Renne, P.R., and Wijbrans, J.R., 2008: Synchronizing rock clocks of Earth history, Science, v. 320, p. 500–504.
Nagorsen-Rinke, S., Lee, J., and Calvert, A., 2013, Pliocene sinistral slip across the Adobe Hills, eastern California–western Nevada: Kinematics of fault slip transfer across the Mina

[1]Supplemental File. Provides a description of $^{40}Ar/^{39}Ar$ analytical techniques, $^{40}Ar/^{39}Ar$ analytical results, and includes supporting age spectra and probability density plots of ages. Please visit https://doi.org/10.1130/GEOS.S.12498308 to access the supplemental material, and contact editing@geosociety.org with any questions.

Downloaded from http://pubs.geoscienceworld.org/gsa/geosphere/article-pdf/16/5/1249/5148564/1249.pdf
by University of Nevada Reno user

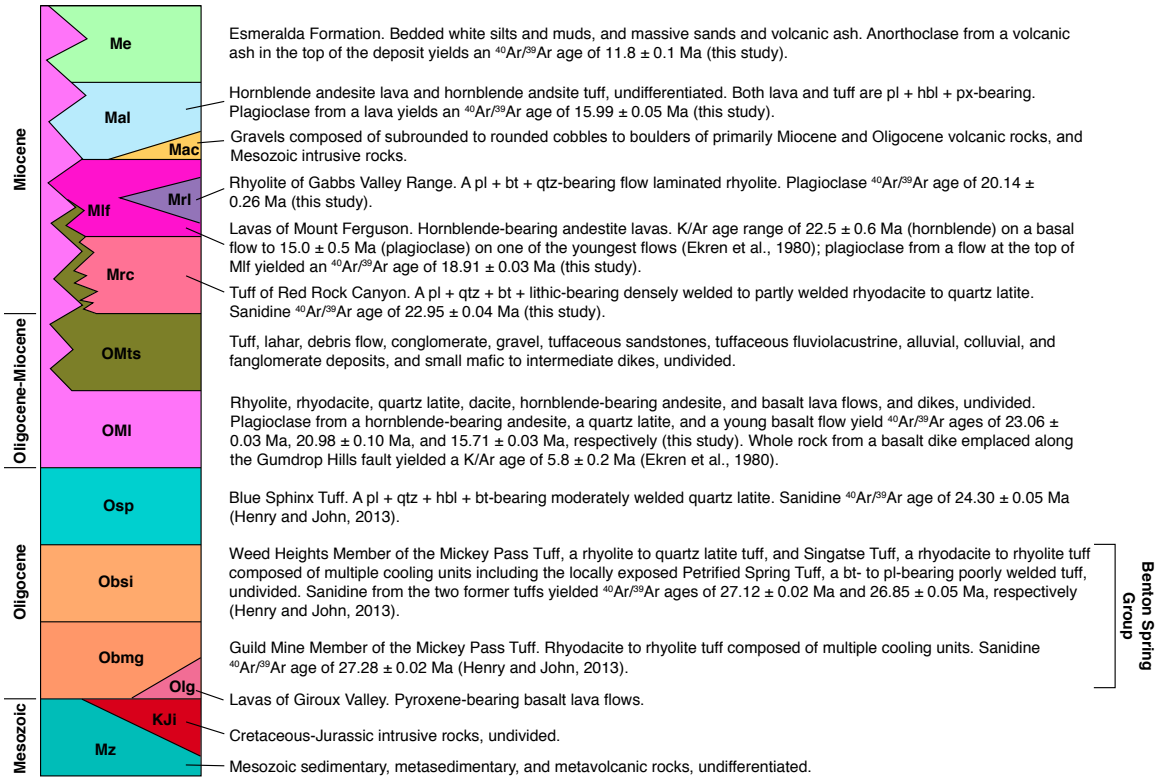

Phenocryst mineral abbreviations: bt, biotite; hbl, hornblende; pl, plagioclase; px, pyroxene; qtz, quartz.

Figure 4. A composite stratigraphic column for the Gabbs Valley and Gilles ranges, Nevada. Sources for stratigraphic data: Ekren and Byers (1985a, 1985b, 1986a, 1986b); Hardyman (1980); Hoxey et al. (2020); this study.

rhyodacite tuffs of varying composition and texture, unconformably overlie unit Olg and Mesozoic basement (Figs. 3 and 4). The stratigraphically lowest tuff in the Benton Spring Group is the Guild Mine Member of the Mickey Pass Tuff, a 27.24 ± 0.04 Ma (sanidine $^{40}Ar/^{39}Ar$ age; Henry and John, 2013) rhyodacite to rhyolite. Younger tuffs in the Benton Spring Group include unit Obsi, composed of the rhyolite to quartz latite 27.12 ± 0.02 Ma (sanidine $^{40}Ar/^{39}Ar$ age of; Henry and John, 2013) Weed Heights Member of the Mickey Pass Tuff, the rhyodacite to rhyolite 26.85 ± 0.02 Ma (sanidine $^{40}Ar/^{39}Ar$ age; Henry and John, 2013) Singatse Tuff, and the poorly welded, undated Petrified Spring Tuff.

Exposed unconformably atop the Benton Spring Group is the areally extensive Blue Sphinx Tuff (Osp), a moderately welded quartz latite that yielded a sanidine $^{40}Ar/^{39}Ar$ age of 24.30 ± 0.02 Ma (Henry and John, 2013) (Figs. 3 and 4).

Unit OMl is exposed unconformably atop unit Osp, is interlayered with volcanic and sedimentary deposits (unit OMts; see below), and is composed of lavas and dikes that range in composition from basalt to rhyolite (Figs. 3 and 4). Plagioclase from one of the old hornblende-bearing andesite lavas, a quartz latite lava, and a young basalt flow yield $^{40}Ar/^{39}Ar$ geochronology ages of 23.06 ± 0.03 Ma, 20.98 ± 0.10 Ma, and 15.71 ± 0.03 Ma, respectively (this study), and whole rock from a basalt dike emplaced along the Gumdrop Hills fault yielded a K/Ar age of 5.8 ± 0.2 Ma (Ekren et al., 1980).

Interfingered with and overlying the OMl lavas and the Lavas of Mount Ferguson (unit Mlf; see below), and often in direct unconformable contact with the Benton Spring Group, is unit OMts composed of tuff, lahar, and sedimentary deposits, undifferentiated (Figs. 3 and 4). Locally exposed within these deposits are small mafic and intermediate dikes.

Overlying the older OMl lavas, and often in direct unconformable contact with the Benton Spring Group, is the rhyodacite to quartz latite Tuff of Redrock Canyon (Mrc) (Figs. 3 and 4). Sanidine from this unit yields an $^{40}Ar/^{39}Ar$ age of 22.95 ± 0.04 Ma (this study).

Unconformably overlying units Mrc and the Benton Spring Group, and interfingered with some lavas and sediments in units OMl and OMts, respectively, are the hornblende andesite Lavas of Mount Ferguson (Mlf) (Figs. 3

Downloaded from http://pubs.geoscienceworld.org/gsa/geosphere/article-pdf/16/5/1249/5148564/1249.pdf
by University of Nevada Reno user

TABLE 1. NEW AND PUBLISHED $^{40}Ar/^{39}Ar$ GEOCHRONOLOGY AGES

Unit and/or lithology	Map unit	Sample number	Latitude	Longitude	Mineral	Age ± error (Ma)	Comments
Esmeralda sands volcanic ash	Me	PSF17077A	38.66507	–118.07804	Anorthoclase	11.8 ± 0.1	Total fusion age (weighted mean 23 of 24 grains)
Young basalt lava flow	OMl	PSF17052	38.52970	–117.98078	Groundmass	15.71 ± 0.03	WMPA§
Andesite lava	Mal	BS8	38.57867	–118.07466	Plagioclase	15.99 ± 0.05	WMPA§
Lavas of Mount Ferguson	Mlf	PSF17077B	38.66404	–118.09035	Plagioclase	18.91 ± 0.03	WMPA§
Rhyolite of Gabbs Valley Range	Mrl	BS10	38.65639	–118.24067	Anorthoclase	20.14 ± 0.26	Total fusion age (weighted mean 10 of 10 grains)
Quartz latite flow	OMl	BS6	38.70553	–118.29729	Anorthoclase	20.98 ± 0.10	Total fusion age (weighted mean 9 of 10 grains)
Tuff of Red Rock Canyon	Mrc	BS4	38.66201	–118.23448	Sanidine	22.95 ± 0.04	Total fusion age (weighted mean 10 of 10 grains)
Hornblende andesite lava	OMl	BS5	38.72236	–118.30496	Plagioclase	23.06 ± 0.03	WMPA§
Blue Sphinx Tuff	Osp	—	—	—	Sanidine	24.30 ± 0.02‡	n = 2*
Singatse Tuff	Obsi	—	—	—	Sanidine	26.85 ± 0.02‡	n = 2*
Weed Heights Member of the Mickey Pass Tuff	Obsi	—	—	—	Sanidine	27.12 ± 0.02‡	n = 2*
Guild Mine Member of the Mickey Pass Tuff	Obmg	—	—	—	Sanidine	27.28 ± 0.02‡	n = 8*

Notes: New samples reported herein were irradiated at the U.S. Geological Survey, Denver, Colorado, USA, Training, Research, General Atomics (TRIGA) reactor using the Taylor Creek sanidine at 28.444 Ma (Fleck et al., 2019) as a neutron flux monitor. This standard age is equivalent to the Fish Canyon sanidine age of 28.198 Ma calibrated to the astronomical age of the Melilla tephra (Kuiper et al., 2008). Plateau ages are defined by a consecutive series of steps where ≥50% of ^{39}Ar released is within error. Latitude and longitude recorded in the World Geodetic System 1984.

§WMPA—weighted mean plateau age.

‡Henry and John (2013).

*n—number of dated samples.

and 4). $^{40}Ar/^{39}Ar$ geochronology on plagioclase from a lava flow near the top of unit Mlf yields an age of 18.91 ± 0.03 Ma (this study). Ekren et al. (1980) reported a K/Ar age range for these lavas of 22.5 ± 0.6 Ma on hornblende from a basal flow and 15.0 ± 0.5 Ma on plagioclase from one of the youngest flows.

Interbedded within Mlf in eastern part of the Gabbs Valley Range and crosscutting as a dome structure in other localities is the flow-laminated, biotite-bearing Rhyolite of Gabbs Valley Range (Mrl) (Figs. 3 and 4). Plagioclase from this unit yields an $^{40}Ar/^{39}Ar$ geochronology age of 20.14 ± 0.26 Ma (this study).

In the southeastern part of the map area, unit Mac, composed of subrounded to rounded cobble to boulder-sized clasts of Mesozoic granitoids and Oligocene and Miocene volcanic rocks, nonconformably overlies the Mesozoic basement (Figs. 3 and 4). Given the volcanic clasts are likely sourced from the Benton Spring Group volcanic rocks and Mlf lavas (Hoxey et al., 2020), unit Mac likely filled a basin that developed adjacent to Mount Ferguson after emplacement of unit Mlf. Emplaced on top of unit Mac and Mesozoic units is the hornblende-bearing andesite lava unit Mal; plagioclase from this unit yields an $^{40}Ar/^{39}Ar$ geochronology age of 15.99 ± 0.05 Ma (this study) (Figs. 3 and 4). Interbedded with unit Mal is a lithic-rich hornblende-bearing andesite tuff.

The Esmeralda Formation, unit Me, composed of diatomaceous muds, silts, sands, and volcanic ash, overlies and is interbedded with unit Mlf, and unconformably overlies Oligocene units Olg and Obmg (Figs. 3 and 4). Anorthoclase from a volcanic ash near the top of the unit yields an $^{40}Ar/^{39}Ar$ geochronology age of 11.8 ± 0.1 Ma (this study).

In the Wassuk Range, we show unit MzC, which is composed of undifferentiated Mesozoic metasedimentary and intrusive rocks and undifferentiated Cenozoic sedimentary and volcanic rocks, with the exception of unit Obmg.

FAULT GEOMETRY, GEOMORPHOLOGY, AND KINEMATICS

Six primary NW-SE–striking, near-vertical dextral faults are exposed in the GVGR. We divide these six faults into four relatively long (~25–55 km) faults, the Petrified Spring, Benton Spring, Gumdrop Hills, and Agai Pah Hills faults, and two relatively short (~5–12 km) faults, the Radio Tower and the Indian Head faults (Fig. 3). All faults cut pre-Quaternary units, are relatively well defined geomorphically, and are characterized by a primary fault trace and, locally, one or more splays (Fig. 3). All faults, except the Radio Tower fault, expose fault scarps developed in Pleistocene alluvial deposits. Tectonic geomorphic features along these faults include alternating scarp facing directions, shutter ridges, dextrally offset channels and alluvial fan surfaces, vegetation lines, and alignment of springs in alluvial deposits (Wesnousky, 2005; Angster et al., 2019; Langille et al., 2016, 2018; this study).

The longest of the faults, the Petrified Spring, Benton Spring, and Gumdrop Hills faults, and one of the shorter faults, the Indian Head fault, strike subparallel to 323°, the SN-CGB motion azimuth. In contrast, the Radio Tower and Agai Pah Hills faults strike ~330°–348°, an azimuth range that is more northerly with respect to the SN-CGB motion azimuth (Fig. 3). The Radio Tower fault cannot be traced northward into Win Wan Flat or southward into Soda Spring Valley (Fig. 3) (Ekren and Byers, 1985b; this study). We interpret these field observations, along with its ~340° average strike relative to the ~323° strike of longer Gumdrop Hills fault, as indicating that slip along the Radio Tower is transferred northward onto the Gumdrop Hills fault.

The Indian Head and Agai Pah Hills faults define an en echelon, left-stepover geometry across the southeastern part of the Gillis Range, which is underlain

Downloaded from http://pubs.geoscienceworld.org/gsa/geosphere/article-pdf/16/5/1249/5148564/1249.pdf
by University of Nevada Reno user

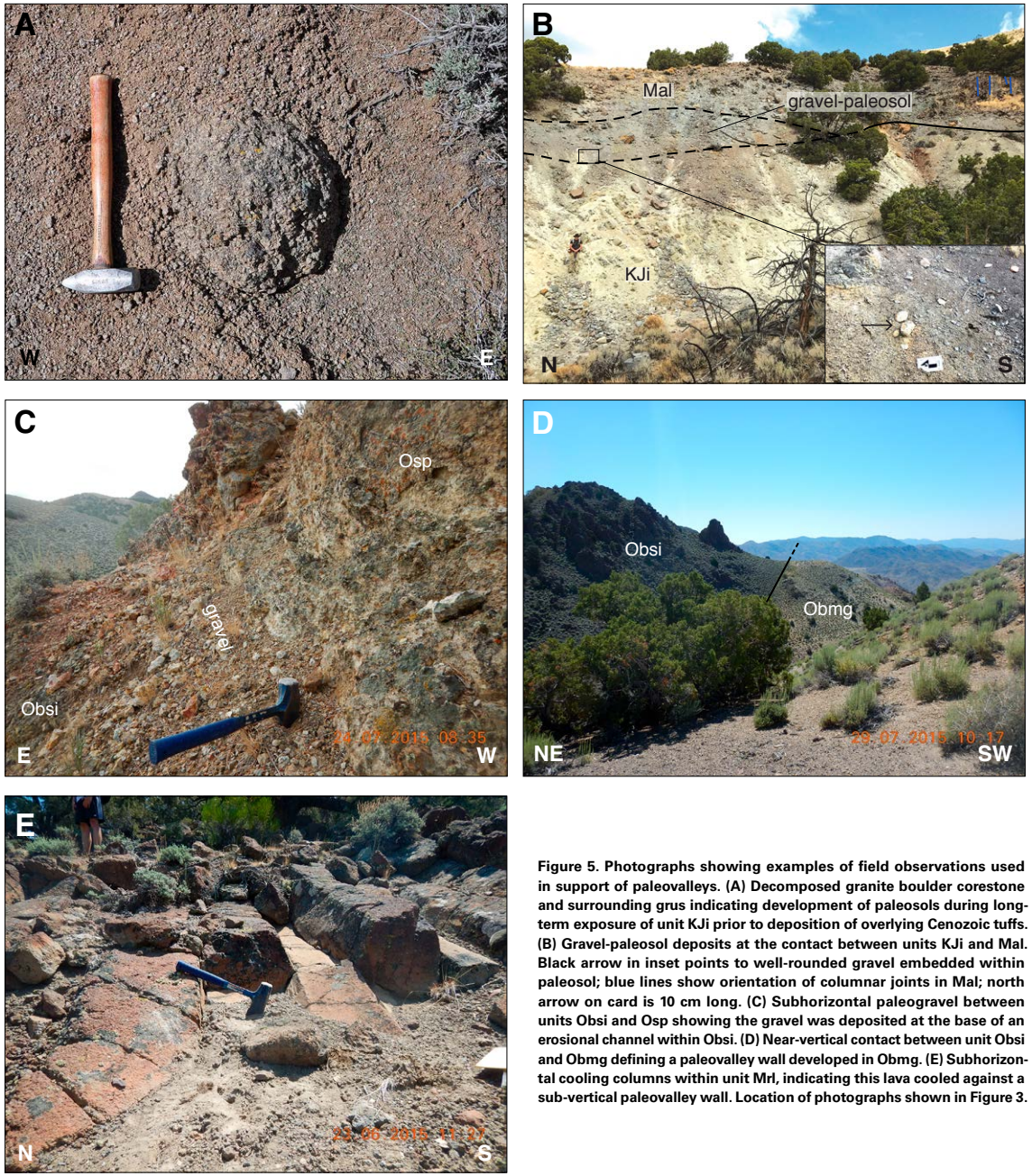

Figure 5. Photographs showing examples of field observations used in support of paleovalleys. (A) Decomposed granite boulder corestone and surrounding grus indicating development of paleosols during long-term exposure of unit KJi prior to deposition of overlying Cenozoic tuffs. (B) Gravel-paleosol deposits at the contact between units KJi and Mal. Black arrow in inset points to well-rounded gravel embedded within paleosol; blue lines show orientation of columnar joints in Mal; north arrow on card is 10 cm long. (C) Subhorizontal paleogravel between units Obsi and Osp showing the gravel was deposited at the base of an erosional channel within Obsi. (D) Near-vertical contact between unit Obsi and Obmg defining a paleovalley wall developed in Obmg. (E) Subhorizontal cooling columns within unit Mrl, indicating this lava cooled against a sub-vertical paleovalley wall. Location of photographs shown in Figure 3.

Downloaded from http://pubs.geoscienceworld.org/gsa/geosphere/article-pdf/16/5/1249/5148564/1249.pdf
by University of Nevada Reno user

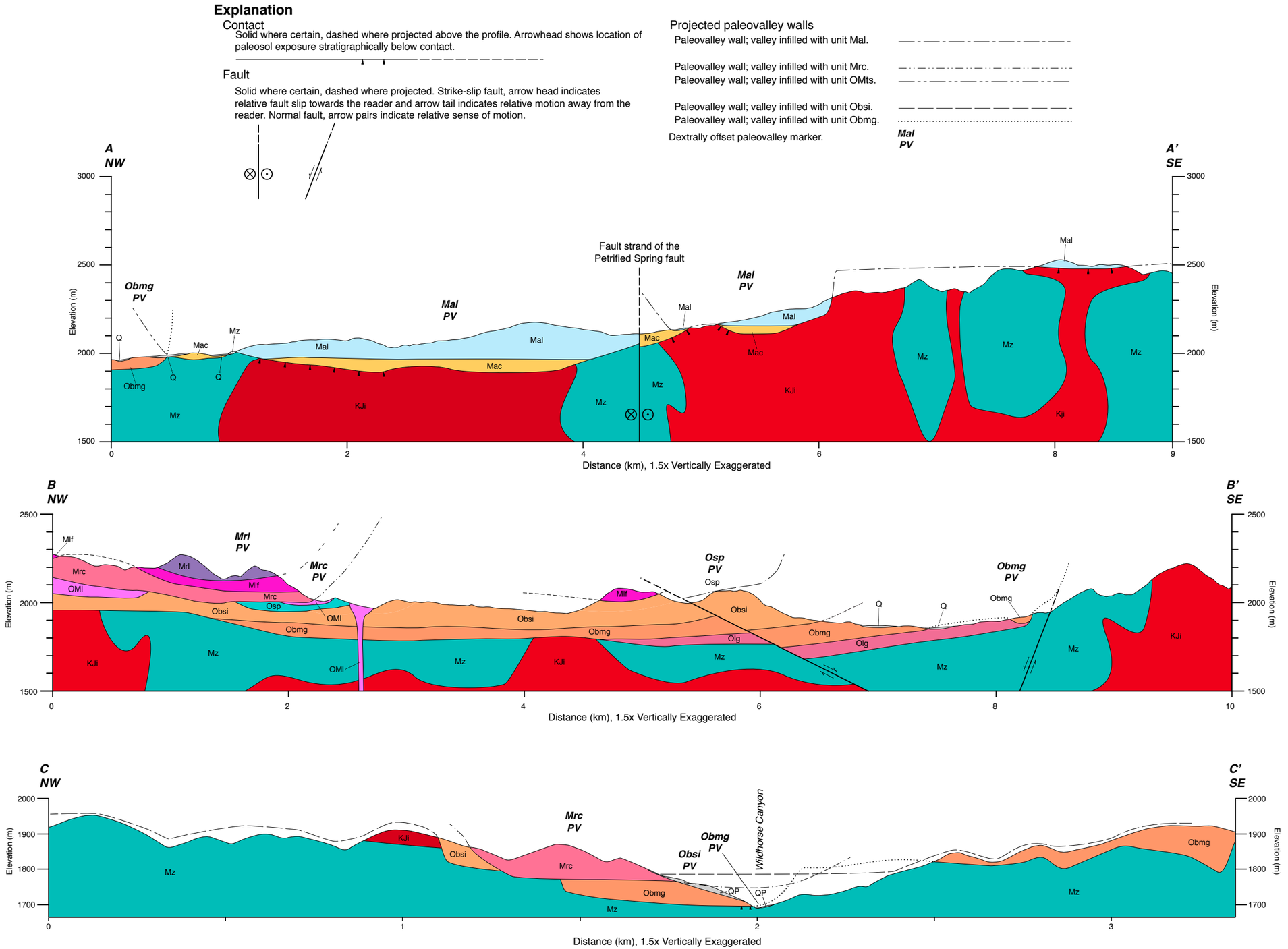

Figure 6. Interpretative cross sections illustrating the cross-sectional geometry of several paleovalleys. See Figure 3 for location of all cross sections and Figure 8 for location of cross section CC′. Cross sections AA′ and BB′ are plotted at the same scale, and cross section CC′ is plotted at a smaller scale. Figure 6 is intended to be viewed at a width of 45.1 cm. To view Figure 6 at this size, please visit https://doi.org/10.1130/10.1130/GEOS.S.12501158.

Figure 6 is intended to be viewed at a width of 45.1 cm. To view Figure 6 at this size, please visit https://doi.org/10.1130/GEOS.S.12501158.

Downloaded from http://pubs.geoscienceworld.org/gsa/geosphere/article-pdf/16/5/1249/5148564/1249.pdf
by University of Nevada Reno user

by extensive exposures of Mesozoic sedimentary, volcanic, and intrusive rocks (Fig. 3). We postulate that the en echelon fault geometry defines a restraining (contractional) stepover in a dextral fault system. To confirm this interpretation, detailed mapping of this region, centered on identifying common features observed in contractional stepovers, such as thrust faults, push-up ridges, and positive flower structures (e.g., Cunningham and Mann, 2007), is needed.

Geomorphically, each fault is typically expressed at the surface as a single linear, seasonally active erosional channel. In addition, lithologic contact geometries, scarce travertine deposits, and along the Petrified Spring fault, strongly folded and upturned lacustrine sediments of the Esmeralda Formation, are strong indicators of the fault's location. Along the trace of these faults, exposures of the fault planes are not common. We observed several narrow (cm to m scale) zones of fault gouge and breccia along most of the faults and a few 10–500-m-wide by 500–1500-m-long zones of red fault gouge and breccia, composed of cobble and boulder-sized clasts, along the Benton Spring and Gumdrop Hills faults. Only a few measurable fault planes and associated fault striations on fault splays were observed along the Petrified Spring, Gumdrop Hills, and Indian Head faults. The fault striations on the Petrified Spring and Gumdrop Hills faults record a shallow plunge (02°–28°) toward the southeast, indicating dominantly strike-slip motion. A fault striation on a splay of the Indian Head fault records a moderate plunge (46°) to the northwest, indicating oblique normal-dextral slip.

A number of field observations along the six faults, including alternating fault-scarp face directions along strike, termination of E-W– and NW-SE–trending valleys and ridges at the fault trace, sub-vertical fault planes, and linear fault traces across topography, suggest dominantly strike-slip motion along these faults.

MAGNITUDE OF DEXTRAL OFFSET AND FAULT-SLIP RATES

Documentation of the magnitude and timing of dextral offset and fault-slip rates across the central Walker Lane are critical for evaluating the space-time patterns of faulting, and to compare these space-time patterns to the forces that drive faulting. We address these issues below by first summarizing the results of earlier work on the magnitude of offset across the dextral faults, and then, based on our detailed geologic mapping, structural, and geochronology studies, describing offset geologic markers, their magnitude of dextral offset, and fault-slip rates.

Previous Work

Prior work in the GVGR centered on geologic mapping (Ekren and Byers, 1985a, 1985b, 1986a, 1986b; Stewart et al., 1981; Hardyman, 1980) and using Mesozoic and Cenozoic markers to document the magnitude of dextral offset across the faults. Across the Petrified Spring fault, Ekren and Byers (1984) used the regional distribution of the Oligocene Benton Spring Group to speculate that the Petrified Spring fault recorded ~16 km of dextral offset since emplacement of those tuffs. In contrast, Hardyman et al. (2000) used the distribution of the Oligocene–early Miocene tuff of Toiyabe to suggest a much larger dextral offset, as much as 35 km, along the Petrified Spring fault and 10–15 km of dextral slip since emplacement of middle Miocene lava flows.

Across the southern Benton Spring fault, Nielsen (1965) suggested that a range of Mesozoic age markers exposed in the Garfield Hills on the west side of the southern Soda Spring Valley were also exposed on the east side of the valley in the Pilot Mountains, but farther south, indicating dextral offset of ~6.5–18.0 km (Fig. 2). Along the Benton Spring fault exposed in the Gabbs Valley Range, Ekren and Byers (1984) argued that a steep intrusive contact between Mesozoic granitic rocks and Mesozoic metasedimentary rocks was dextrally offset 6.4–9.6 km and that Tertiary tuffs were dextrally displaced ~8 km. Ekren et al. (1980) suggested that the southern limit of the exposed late Oligocene Blue Sphinx Tuff was dextrally offset ~9 km across the Benton Springs fault.

Based on mapping along the northern part of the Gumdrop Hills fault in the Gillis Range, Hardyman (1978, 1980) suggested that the Cretaceous granite of Red Granite Mine was dextrally offset ~6.4 km. Along the southern part of the Gumdrop Hills fault in the Gabbs Valley Range, Ekren and Byers (1984) interpreted steeply dipping Triassic sedimentary rocks exposed on both sides of the fault as recording ~9 km of dextral offset.

Ekren and Byers (1984) used a steeply dipping marker bed in the Triassic Luning Formation to measure slightly more than 4 km of dextral offset across the Indian Head fault. To our knowledge, no one has published dextral offset measurements across the Agai Pah Hills fault. None of these research groups described the offset geologic markers in detail (e.g., exact location, geometry, and well-constrained age).

Geologic Markers and Evidence for Paleovalleys

Based on our geologic mapping and structural studies and reinterpretation of published geologic maps (Ekren and Byers, 1985a, 1985b, 1986a, 1986b; Stewart et al., 1981; Hardyman, 1980), we identified eight geologic markers, including six Cenozoic tuff- and lava-filled paleovalleys, the southern edge of the Lavas of Mount Ferguson (unit Mlf), and a line defined by the intersection of a normal fault and the horizontal contact between unit Me overlying unit Mlf, to measure the magnitude of offset across the major dextral faults in the Gabbs Valley Range (the Petrified Spring, Benton Spring, and Gumdrop Hills faults) (Figs. 2 and 3). We use near-vertical contacts between Mesozoic units to document dextral offset across the Radio Tower and Indian Head faults. Based on published geologic maps (Ekren and Byers, 1985b; Hardyman, 1980), we interpret the westward continuation of two Cenozoic volcanic-filled paleovalley markers to measure dextral offset across the Agai Pah Hills fault, Gillis Range (Figs. 2 and 3).

Downloaded from http://pubs.geoscienceworld.org/gsa/geosphere/article-pdf/16/5/1249/5148564/1249.pdf
by University of Nevada Reno user

Our field observations along the contact between Mesozoic and Cenozoic units show the development of paleosols, composed of gravel deposits, grus, granitoid corestones, and heavily fractured intrusive rocks (Figs. 5A and 5B). We also observe paleosol and gravel deposits locally along some of the Cenozoic contacts (Fig. 5C). These observations, along with the broad "U"-shaped geometry in cross section of these contacts (Fig. 6) and their sublinear map geometry (Fig. 3), lead us to interpret them as unconformities that define sub-linear paleovalleys incised into Mesozoic basement and Cenozoic units and subsequently infilled with Cenozoic volcanic rocks. Our interpretation is in contrast to that of Ekren and Byers (1985a, 1985b, 1986a, 1986b) and Hardyman (1980), who suggested that most of these contacts were low-angle normal faults. These ~1–5-km-wide, gravel and paleosol-floored paleovalleys, channeled flow of volcanic material and define sub-linear geologic markers that were truncated by subsequent dextral faulting (Figs. 3 and 6). Below we describe the field relations and geometry of the six volcanic-filled paleovalleys and use the better exposed paleovalley wall to interpret the map trace of these paleovalleys.

The oldest paleovalley that we mapped, extending from east of the Petrified Spring fault to west of the Gumdrop Hills fault, consists of a series of nested approximately E-W–trending, ~2–4-km-wide, lava- and tuff-filled paleovalleys incised into Mesozoic metasedimentary and intrusive rocks (Figs. 3 and 6). Based on our interpretation of published geologic maps (Ekren and Byers, 1985b; Hardyman, 1980), we extend this paleovalley to the west of the Agai Pah Hills fault. On the east side of the Petrified Spring fault, unit Olg infilled a valley incised into Mesozoic units, defining a ≥1-km-wide, ≥50-m-deep paleovalley, that was subsequently incised, and largely eroded away, before being infilled with two tuffs, the 27.28 ± 0.02 Ma Obmg (maroon marker line in Fig. 3) and the 26.85 ± 0.05 Ma Obsi (part of the Benton Spring Group), defining an ~4-km-wide, up to ~1-km-deep paleovalley. This repeated incision and tuff emplacement, which results in the nested geometry schematically illustrated in Figure 7, has been observed elsewhere in the Great Basin (e.g., Henry et al., 2012; Colgan and Henry, 2017). The nested geometry suggests a long-standing drainage network characterized by deposition and erosion that lasted hundreds of thousands to millions of years. The result that we observe today is significant lateral variation in unit thickness, nonlinear exposures of some paleovalley infilling units, and locally poorly exposed to non-exposed paleovalley walls.

On the west side of the Petrified Spring fault, southwest of Calvada Flat, the southern boundary of the nested paleovalley series filled with Benton Spring Group tuffs is well defined by a steeply north-dipping, E-W–striking normal fault developed in the Mesozoic basement; the northern paleovalley wall is obscured by the overlying younger Mrc and Mlf (Fig. 3). The base of this nested paleovalley series is also well defined on either side of the Benton Spring fault by a grus deposit surrounding ≤1.5-m-size spheroidal weathered corestones developed in the Mesozoic granitic rocks that underlie the unconformity (Fig. 5A). The northern boundary of this part of the paleovalley is buried beneath tuffs and lava flows younger than the Benton Spring Group.

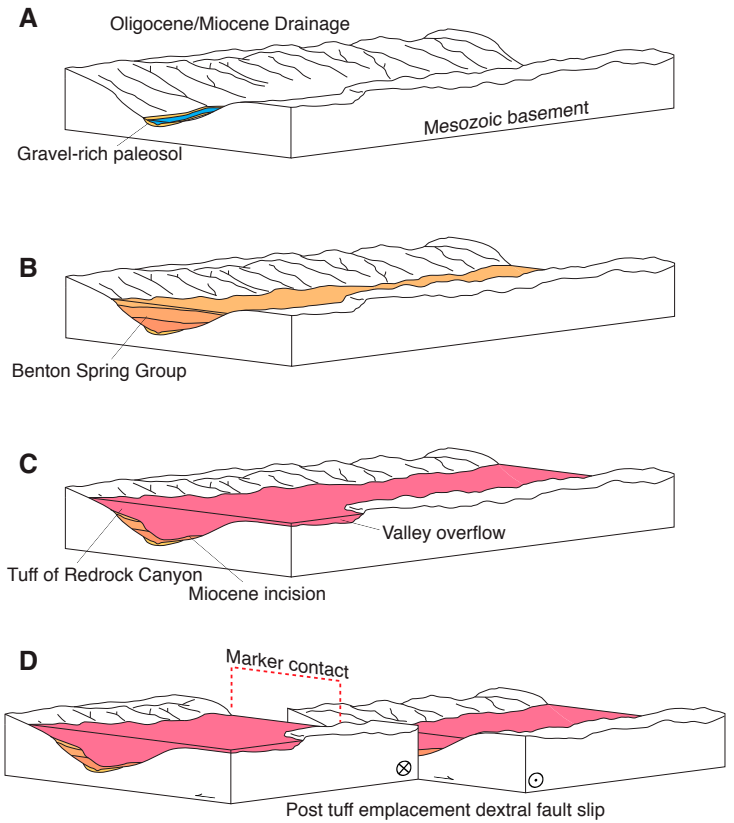

Figure 7. Schematic block model representation of paleovalley evolution. (A) Early Cenozoic valley incision and gravel-rich paleosol development on Mesozoic basement. (B) Volcanic eruption and emplacement of valley-filling tuffs (e.g., Oligocene Benton Spring Group). (C) Continued incision into Oligocene tuffs and subsequent filling with Miocene volcanic rocks creates nested paleovalley geometry. Constraints on valley width can be obscured by valley overflow. (D) Steep-sided walls of paleovalleys act as a geologic marker across a dextral fault.

The southern wall of this paleovalley is well exposed between the Benton Springs fault to the east and the Gumdrop Hills fault to the west. Westward from the Gumdrop Hills fault to the Agai Pah Hills fault, across Win Wan Flat, Win Wan Valley, and Buckley Flat, the southern wall of this paleovalley is mostly inferred beneath Quaternary deposits but is reasonably well exposed to the west of the Agai Pah Hills fault (Fig. 3).

A second paleovalley was incised into the Benton Spring Group tuffs and subsequently was infilled with the 24.30 ± 0.05 Ma unit Osp (defining an ~1-km-wide, ~50-m-thick paleovalley) (dark-blue marker in Fig. 3). East of the Benton Spring fault, the southern paleovalley wall is approximately vertical

Downloaded from http://pubs.geoscienceworld.org/gsa/geosphere/article-pdf/16/5/1249/5148564/1249.pdf
by University of Nevada Reno user

(Fig. 5D), whereas the northern wall is buried beneath younger deposits. Farther to the east, within 5 km west of the Petrified Spring fault, this paleovalley is not exposed, and we did not observe exposures of Osp on the east side of this fault. Between the Benton Spring and Gumdrop Hills faults, the northern and southern walls of the paleovalley are poorly exposed. In one locality, the exposed northern wall is vertical, whereas the southern wall is either buried beneath younger lava flows or eroded away. The westward continuation of the southern wall of this paleovalley between the Gumdrop Hills and Agai Pah Hills faults and to the west of the latter fault is mostly inferred because unit Osp is poorly exposed.

A third paleovalley was incised into the Benton Spring Group, the Blue Sphinx Tuff, and some older lavas, and then infilled with the 22.95 ± 0.04 Ma Tuff of Red Rock Canyon (Mrc) (defining an ~1–3-km-wide, ~300-m-thick paleovalley). This paleovalley is observed from the east side of the Benton Spring fault to the west side of the Gumdrop Hills fault (red marker in Fig. 3) (Figs. 6, 8, and 9). To the east of the Benton Spring fault, two southern paleovalley walls are moderately to well exposed and define two paleovalleys. The northern walls of both paleovalleys are either covered by the unit Mlf, in high- to moderate-angle depositional contact on top of older OMl, or in low-angle depositional contact with the underlying unit OMts. The map traces of the southern walls of the two paleovalleys are different—the southern paleovalley wall of the southern paleovalley trends NW-SE, whereas the southern paleovalley wall of the northern paleovalley trends NE-SW. Between the Benton Spring fault and the Gumdrop Hills fault, both the north and south walls of the Mrc-infilled paleovalley are well exposed in Wildhorse Canyon[2], defining the best preserved paleovalley in the field area (Figs. 3, 6, 8, and 9). This NE-SW–trending paleovalley was incised into units Obmg and Obsi, which in turn were deposited nonconformably on Mesozoic basement that defined a topographic high. The dip of both valley walls ranges from steep, to moderate, to shallow. On the west side of the Gumdrop Hills fault, the paleovalley infilling unit, Mrc, is exposed only in a small outcrop (~250 m^2) surrounded by Pliocene–Quaternary alluvial fan deposits located on the north side of the western end of Nugent Wash (Fig. 3). Units Obmg, Obsi, Osp, and OMl are exposed to the north and south of this small outcrop of Mrc (Fig. 3), a geologic relationship that we also observe, but is considerably better exposed, in the Wildhorse Canyon area on the east side of the Gumdrop Hills fault (Fig. 8). We interpret the exposures of these older units in the Nugent Wash region as defining the locations of the inferred maximum northern and southern paleovalley walls of the NE-SW–trending Mrc-infilled paleovalley.

Poorly exposed on the east and west sides of the Petrified Spring and Benton Spring faults is a fourth paleovalley, which incised into several units including Obsi, Osp, Mrc, and older flows within Mlf, and was subsequently infilled with the 20.14 ± 0.26 Ma Rhyolite of Gabbs Valley Range (unit Mrl; dark-green marker in Fig. 3) (Fig. 5E).

[2]This is the Wildhorse Canyon of the Gabbs Valley Range, not the Wildhorse Canyon of the Gillis Range.

Along the southeastern end of the Petrified Spring fault is the fifth paleovalley, which incised into Mesozoic rocks and was subsequently infilled first with unit Mac, a locally preserved, thin (≤40 m) gravel deposit composed primarily of rounded and subrounded clasts of Mesozoic intrusive rock and Miocene and Oligocene volcanic rock and secondly with at least ~200 m of the overlying 15.99 ± 0.05 Ma unit Mal (dark-orange marker in Fig. 3) (Fig. 6). Where these Cenozoic units nonconformably overlie Mesozoic intrusive rock, the contact is often characterized by ~2-m-thick grus deposits surrounding ≤1.5-m-size spheroidal weathered corestones developed within the intrusive (Fig. 5B). At the northwestern exposures of unit Mal, the basal contact is subhorizontal with broad (~100 m length, ~10 m height) undulations and is commonly found partially underlain with the gravel deposit. The abundance of rounded and subrounded clasts and geometry of the contact with the underlying Mesozoic units suggest that the gravel was deposited within an east-west–trending fluvial paleovalley that broadens (~2–4 km) from east to west. Our interpretation is in contrast to that of Ekren and Byers (1985a), who suggested that the gravel is a remnant alluvial fan deposit. In the deepest segments of this paleovalley, we observe ≤100-m-thick deposits of a hornblende-bearing tuff. In a densely welded portion of this tuff, columnar joints form an ~15-m-wide rosette pattern, which we suggest is the result of evacuation of superheated fluids during tuff emplacement over an active fluvial environment (e.g., Wright et al., 2011). Where unit Mal is observed in direct contact with the Mesozoic basement west of the Petrified Spring fault, it is typically found in near-vertical contact, suggesting the presence of a steep-sided canyon partially filled with gravel deposits during emplacement of unit Mal. In contrast, the southernmost contact between Mal and Mesozoic rocks east of the Petrified Spring fault is subhorizontal, and the basal, platy jointed sections of unit Mal are not present. We interpret the near-vertical paleovalley wall contact as part of a narrow (~1 km) portion of the paleovalley and the southernmost exposures as evidence that unit Mal filled the paleovalley before overflowing onto an adjacent floodplain.

The youngest paleovalley identified, which is only exposed in the southeastern part of the map area (Fig. 3), is incised into lacustrine sediments of unit Me, and infilled with a 15.71 ± 0.03 Ma basalt lava flow (the youngest basalt flow in unit OMl). The contact shows an arcuate, concave-up geometry and columnar joints in the overlying basalt lava form a radial pattern (Fig. 10A). A pole to the best-fit circle of the measured, radially oriented columnar joints yields a 63° trend for the axis of arcuate contact (Fig. 10B). We interpret the radial distribution of the columnar joints as indicative of a paleovalley here trending NE-SW.

Dextral Offset Magnitudes and Calculated Slip Rates

Based on our mapping, combined with our interpretation of published geologic maps (Hardyman, 1980; Stewart et al., 1981; Ekren and Byers, 1985a, 1985b, 1986a, 1986b), we identified six Cenozoic markers dextrally offset across the Petrified Spring fault, four across the Benton Spring fault, three across the

Downloaded from http://pubs.geoscienceworld.org/gsa/geosphere/article-pdf/16/5/1249/5148564/1249.pdf
by University of Nevada Reno user

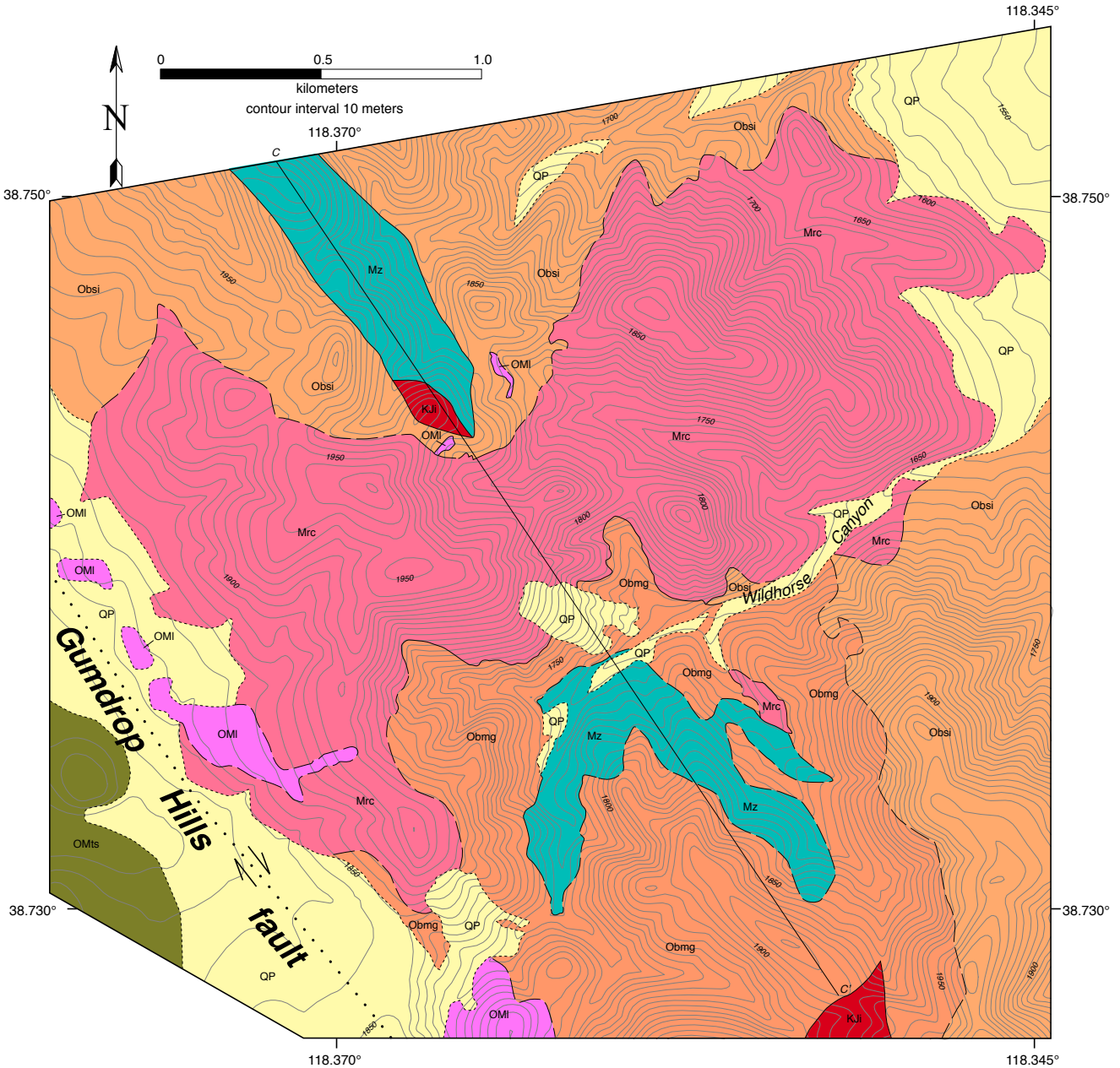

Figure 8. Geologic map of the Wildhorse Canyon area of the Gabbs Valley Range, Nevada. Map shows the NE-SW–trending paleovalley infilled with unit Mrc. For definition of unit labels, unit colors, and contact types, see Figure 3. Cross section CC′ is shown in Figure 6.

Downloaded from http://pubs.geoscienceworld.org/gsa/geosphere/article-pdf/16/5/1249/5148564/1249.pdf
by University of Nevada Reno user

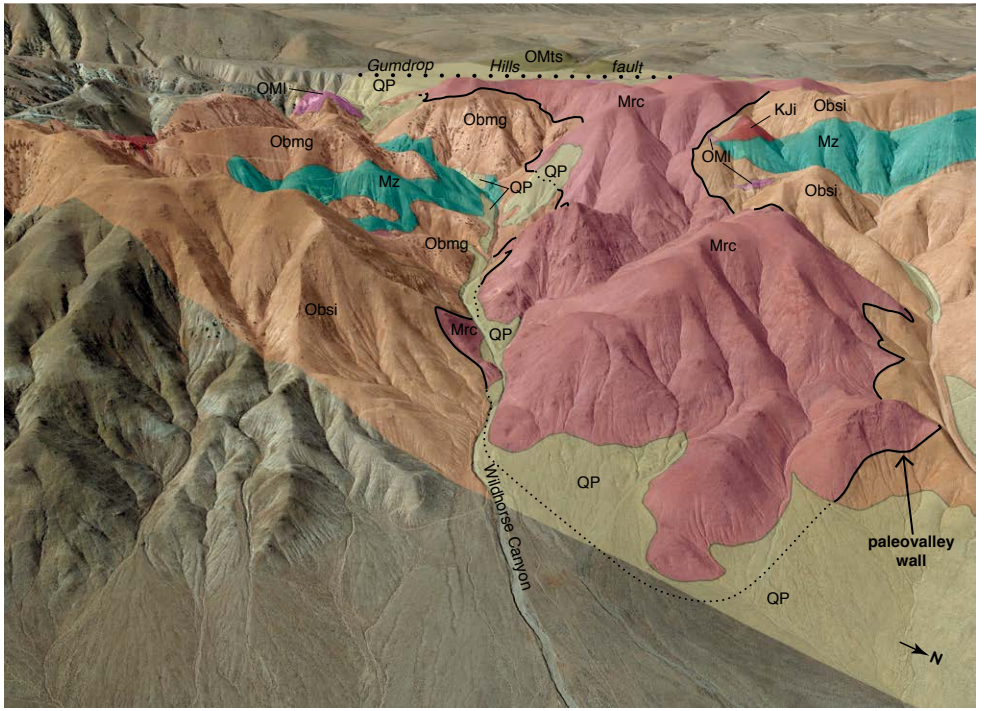

Figure 9. Oblique, 1.5× vertically exaggerated Google Earth image of Wildhorse Canyon with superimposed geology showing the Tuff of Red Rock Canyon infilled paleovalley (see Fig. 8 for Wildhorse geologic map). Vertical thickness of unit Mrc on hill in left foreground is ~300 m. See Figures 3 and 4 for unit abbreviations.

Gumdrop Hills fault, and two across the Agai Pah Hills fault (Fig. 3; Table 2). We did not observe any pre-Quaternary Cenozoic markers offset across the Radio Tower and Indian Head faults, but we identified near-vertical Mesozoic markers to measure dextral offset across these faults.

Similar to studies completed along other faults elsewhere in the Basin and Range (e.g., Proffett and Proffett, 1976; Henry and Faulds, 2010), we use the sub-linear traces of paleovalleys as geologic markers to document dextral offset magnitudes across the four main faults in the GVGR. When using paleovalleys as offset markers, ideally near-vertical paleovalley wall contacts are traced and assumed (unless otherwise noted) to be part of a single throughgoing paleovalley without any bifurcations in the paleo-drainage system; we also assume that the present-day contact orientation is not the result of horizontal axis rotation.

We estimate the uncertainty in the offset magnitude by the length of the estimated projection of the marker's map trend as a horizontal line to the fault trace, the dip of the marker, and the geometry of the offset marker. For well-defined, near-vertical contacts that project within ~100 m to the fault, a minimum 15% uncertainty is assigned; for non-vertical contacts projected over distances greater than 100 m, a minimum 30% uncertainty is assigned; and for contacts buried on one side of the fault, a 50% uncertainty is assigned.

Petrified Spring Fault

Along the Petrified Spring fault, the oldest marker dextrally offset is the series of nested paleovalleys defined by a sub-linear, sub-vertical, nonconformable contact between Oligocene volcanic rocks, the Lavas of Giroux Valley, and the Benton Spring Group tuffs (units Olg, Obmg, and Obsi), deposited against Mesozoic metasedimentary and intrusive rocks. This paleovalley is truncated and dextrally offset by the several splays along the southern section of the Petrified Spring fault into four fault blocks (maroon Obmg marker in Fig. 3). On the west side of the Petrified Spring fault, in the westernmost block, the southern boundary of the nested paleovalley is well defined by a near-vertical contact and projected ~1.5 km to the fault. In contrast, on the east side of the fault, the contact is buried by a Quaternary landslide (Fig. 3). Given these field constraints, we assign a 50% uncertainty to our offset measurement. The measured dextral offset of the Benton Spring Group nested paleovalley is 10.3 ± 5.1 km across all splays of the Petrified Spring fault (Fig. 3; Table 2).

Unit Mrl (dark-green marker in Fig. 3) also exhibits dextral offset across the Petrified Spring fault. On the west side of the fault, isolated outcrops of Mrl unconformably overlie, in near-vertical to subhorizontal contact, units Obsi, Mrc, and locally unit Mlf. On the east side of the fault, small exposures of unit

Downloaded from http://pubs.geoscienceworld.org/gsa/geosphere/article-pdf/16/5/1249/5148564/1249.pdf
by University of Nevada Reno user

Mrl unconformably overlie units Olg and Obmg in shallow to subhorizontal contacts; locally, a paleosol is exposed along these contacts. Given the poor exposure of Mrl, the ~6 km projection of the inferred southern Mrl contact on the west side of the Petrified Spring fault, and the low-angle geometry of this contact on the east side of the fault, we assign an uncertainty of 50% to our offset measurement. Assuming the projection of the exposed southern Mrl contact continues along trend to the fault, then this unit is dextrally offset by 10.0 ± 5.0 km (Fig. 3; Table 2).

Our mapping of the Lavas of Mount Ferguson (unit Mlf) shows an apparent dextral offset of its southern boundary across the Petrified Spring fault (yellow marker in Fig. 3), confirming the mapping of Ekren and Byers (1985a). Given the low-angle geometry of this southern contact, we assign an uncertainty of 50% to our dextral offset measurement magnitude of 10.1 ± 5.1 km (Fig. 3; Table 2).

The fourth geologic marker, a paleovalley infilled with unit Mal, is truncated and dextrally offset into four fault blocks by three main strands along the southern part of the Petrified Spring fault (dark-orange marker in Fig. 3) (Fig. 6). In the middle two blocks, the southern contact of Mal is a well-exposed buttress unconformity against Mesozoic basement rocks along a near-vertical contact, which we interpret as the steep southern paleovalley wall of a relatively narrow (~1–2-km-wide) canyon. In the westernmost and easternmost blocks, we infer the location of this southern paleovalley wall. Summing the offset magnitudes across the three fault splays yields a total dextral offset magnitude of 8.0 ± 1.3 km for this paleovalley (Fig. 3; Table 2).

The fifth, and next-youngest, offset marker documented in this study is a paleovalley filled with a young, 15.71 ± 0.03 Ma basalt flow in unit OMl (Figs. 10A and 10B). The ~15.71 Ma basalt flow outcrops on both sides of two of three fault splays along the southern portion of the Petrified Spring fault. Using the 63° trend of this paleovalley axis (see previous section), we measure 1.9 ± 0.4 km of dextral offset across the across two of the three fault splays (Table 2).

The sixth, and youngest, dextrally offset geologic marker across the Petrified Spring fault is the line defined by the intersection of a NW-striking, NE-dipping normal fault and the subhorizontal contact between unit Mlf and the overlying upper part of the unit Me in the hanging wall (light-blue marker in Fig. 3). Unit Mlf defines the footwall of this fault, and units Mlf, Me, and QP define the hanging wall. Although the fault plane is not exposed, joints in the immediate footwall strike 300°, subparallel to the mapped fault trace, and dip 63° NE, which we infer is subparallel to the dip of the fault. Where unit Mlf is exposed in the hanging wall, we observe paleosol developed stratigraphically on top of it; the paleosol was subsequently overlain by sands and the ca. 11.8 Ma volcanic ash of unit Me. This nonconformable contact in the hanging wall is indicative of a normal fault-bounded basin that is filled with the Miocene Esmeralda Formation. We assign a 50% uncertainty to the dextral offset measurement of 3.5 ± 1.8 km of the intersection line due to its ~1.3-km-long projection northwestward into the Petrified Spring fault (Fig. 3; Table 2).

Across the Petrified Spring fault, the four oldest markers—the ca. 27.1 Ma Obmg, the ca. 20.1 Ma unit Mrl, the ca. 18.9 Ma Mlf, and the ca. 16.0 Ma

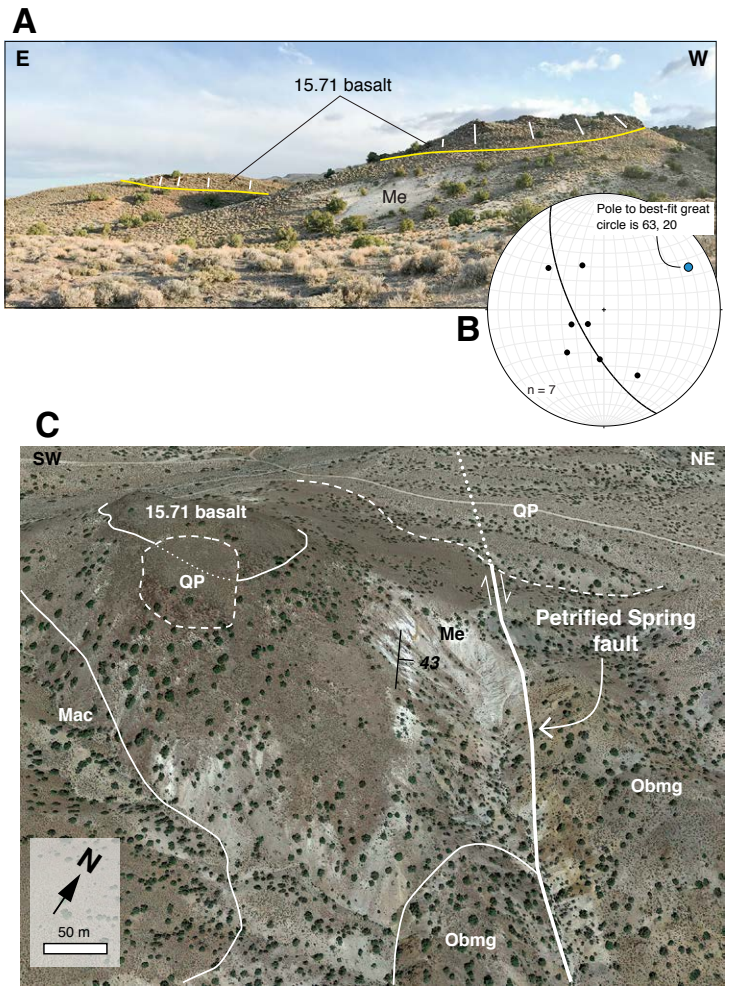

Figure 10. (A) Field photograph of arcuate paleovalley contact between units Me and ca. 15.71 Ma basalt flow in unit OMl. Yellow line shows the trace of the contact between the two units, and white lines show the orientation of columnar joints in the basalt flow, which are perpendicular to the contact. (B) Equal-area stereonet plot of trend and plunge measurements (black dots) collected from cooling-joint intersection lineations at the base of the basalt flow above unit Me. Calculated Bingham best-fit great circle (black line) and pole to that plane (blue dot) to the cooling-joint intersection lineations shown. (C) An oblique, 1.5× vertically exaggerated annotated Google Earth image showing the angular unconformity between the 43° northeast-dipping unit Me and the overlying, subhorizontal ca. 15.71 Ma basalt lava flow of unit OMl. Unit labels and map symbols defined in Figure 3; location of images shown in Figure 3. View to the northwest, approximately along strike of bedding in unit Me.

Downloaded from http://pubs.geoscienceworld.org/gsa/geosphere/article-pdf/16/5/1249/5148564/1249.pdf
by University of Nevada Reno user

TABLE 2. DEXTRAL OFFSET MEASUREMENTS (THIS STUDY)

Marker unit (color)[p]	Age (Ma)	Age source	Dextral offset (km)	Average dextral offset (km)	Average[§] or minimum[a] slip rate (mm/yr)	Slip rate since the middle Miocene (mm/yr)[¥]
Petrified Spring fault						
Unit Obmg (maroon)	27.28 ± 0.02	Henry and John (2013)	10.3 ± 5.1			
Unit Mrl (dark green)	20.14 ± 0.26	This study	10.0 ± 5.0			
Unit Mlf (yellow)	18.91 ± 0.03	This study	10.1 ± 5.1	9.6 ± 1.1	0.4 ± 0.1[§]	0.5 ± 0.1 to 0.6 ± 0.1
Unit Mlf (yellow)	15.0 ± 0.5	Ekren et al. (1980)	10.1 ± 5.1			
Unit Mal (dark orange)	15.99 ± 0.05	This study	8.0 ± 1.3			
Young basalt lava flow (see text Fig. 10) in unit OMl	15.71 ± 0.03	This study	1.9 ± 0.4*	—	—	—
Normal fault cutting the upper Esmeralda Formation (light blue)	11.8 ± 0.1	This study	3.5 ± 1.8	3.5 ± 1.8	0.3 ± 0.2[a]	—
Beheaded channel	0.124 ± 0.006	Angster et al. (2019)	0.0925 ± 0.005[†]	—	—	
Benton Spring fault						
Unit Obmg (maroon)	27.28 ± 0.02	Henry and John (2013)	7.2 ± 1.4			
Unit Osp (dark blue)	24.30 ± 0.05	Henry and John (2013)	4.9 ± 2.5			
Unit Mrc (north paleovalley) (red)	22.95 ± 0.04	This study	9.1 ± 2.7	7.0 ± 1.7	0.4 ± 0.1[a]	0.4 ± 0.1 to 0.5 ± 0.1
Unit Mrc (south paleovalley) (red)	22.95 ± 0.04	This study	12.6 ± 6.3			
Unit Mrl (dark green)	20.14 ± 0.26	This study	6.7 ± 3.3			
Gumdrop Hills fault						
Unit Obmg (maroon)	27.28 ± 0.02	Henry and John (2013)	4.6 ± 2.3	—	—	—
Unit Osp (dark blue)	24.30 ± 0.05	Henry and John (2013)	9.7 ± 4.9			
Unit Mrc (north paleovalley wall) (red)	22.95 ± 0.04	This study	10.7 ± 5.4	9.7 ± 1.0	~0.4[a]	0.6 ± 0.1
Unit Mrc (south paleovalley wall) (red)	22.95 ± 0.04	This study	8.8 ± 4.4			
Radio Tower fault						
Contact between Jurassic sediments and Jurassic granodiorite	—	Ekren and Byers (1985b)	500 ± 50[b]	—	—	—
Indian Head fault						
contact between Triassic Luning Fm. and Jurassic diorite	—	Ekren and Byers (1985b)	5.0 ± 0.5	—	—	—
Agai Pah Hills fault						
Unit Obmg (maroon)	27.28 ± 0.02	Henry and John (2013)	4.1 ± 2.1	4.9 ± 1.1	0.2 ± 0.1[a]	0.3 ± 0.1
Unit Osp (dark blue)	24.30 ± 0.05	Henry and John (2013)	5.6 ± 2.3			

[p]Marker color is that used in text Figure 3.
*Slip measured across two of three fault splays (Fig. 3 in text).
[†]Offset measurement from Angster et al. (2019).
[§]Average slip rate = average dextral offset/age of youngest offset marker; [a]minimum slip rate = dextral offset/age of offset marker.
[¥]Middle Miocene age brackets are 15.99 ± 0.05 Ma to 15.71 ± 0.03 Ma.
[b]Dextral offset measurement is in meters.

Downloaded from http://pubs.geoscienceworld.org/gsa/geosphere/article-pdf/16/5/1249/5148564/1249.pdf
by University of Nevada Reno user

Mal—are dextrally offset 10.3 ± 5.1 km, 10.0 ± 5.0 km, 10.1 ± 5.1 km, and 8.0 ± 1.3 km, respectively (Fig. 3; Table 2). These measured offsets are the same, within error, and as a result, we interpret that average dextral offset of 9.6 ± 1.1 km (one standard deviation) as the best estimate of maximum offset across the Petrified Spring fault that accumulated since 15.99 ± 0.05 Ma, the age the youngest offset marker unit Mal.

Our field observations of unit Me, the 15.71 Ma basalt flow, and the Petrified Spring fault provide a lower bound on the initiation age for fault slip. The ca. 15.71 Ma basalt flow overlies, in an angular unconformity, upturned (dipping 14°–22° to the northeast in Fig. 10A and ~43° to the northeast in Fig. 10C) beds of silt and mud of the lower part of unit Me. This zone of upturned beds in unit Me is subparallel to and in close proximity (within ~200 m) to the Petrified Spring fault. Elsewhere along the Petrified Spring fault, Me beds dip northeast as much as 70°, whereas far from the Petrified Spring fault, Me beds dip 6°–12° eastward. Approximately 400 m south of the field locality shown in Figure 10A and within the Petrified Spring fault zone, we observe an ~10-m-wide zone of broken and shattered Me bedding defining blocks 1–3 m wide and bed tilt orientations in all directions. We interpret these field relations as indicating a period of slip along the Petrified Spring fault; this slip predated emplacement of the ca. 15.71 Ma basalt flow.

Ascribing pre–15.71 Ma deformation of unit Me to normal fault slip and associated northeast tilting along the NW-striking Petrified Spring fault, or some other nearby NW-striking fault, is problematic because units and paleovalleys older than unit Me are not tilted, and unit Me is weakly tilted far from the fault. For example, the base of unit Mlf is subhorizontal and, as noted above, the southernmost exposures of unit Mal are in subhorizontal contact with Mesozoic basement. We suggest that the most viable interpretation of the ~15.71 basalt flow and unit Me field relations (described above and highlighted in Figure 10C) is that the deformation of Me resulted from a combination of the incompetence of the silts and muds that dominate Me, close proximity to the Petrified Spring fault, and dextral slip along the Petrified Spring fault. Thus, these field relationships constrain the timing of deformation of the upturned unit Me beds to between emplacement of unit Mal at 15.99 ± 0.05 Ma and emplacement of the overlying basalt lava flow at 15.71 ± 0.03 Ma. We interpret these relations as indicating a tightly bracketed age for initiation of dextral slip along the Petrified Spring fault of between 15.99 ± 0.05 and 15.71 ± 0.03 Ma. Given these age constraints, the average long-term dextral fault-slip rate is 0.6 ± 0.1 mm/yr along the Petrified Spring fault whether fault slip initiated at ca. 16.0 Ma or at ca. 15.7 Ma.

The NW-trending line defined by the intersection of the NW-striking, NE-dipping normal fault and the subhorizontal contact between unit Mlf and Me along the northern part of the Petrified Spring fault is the youngest pre-Quaternary Cenozoic marker dextrally offset across the Petrified Spring fault (Fig. 3). Dividing the 3.5 ± 1.8 km dextral offset by the 11.8 ± 0.1 Ma volcanic ash from the upper part of unit Me, which provides a maximum age for slip on the normal fault, indicates a minimum post–middle Miocene dextral slip rate of 0.3 ± 0.2 mm/yr (Table 2).

Since the Petrified Spring fault records progressive offset of geologic markers, whereby older markers record larger offsets, another approach to calculating dextral fault-slip rates is to apply a linear regression to age versus dextral offset plots (Fig. 11). In addition to our age and offset magnitude data, we include the dextral offset magnitude for a late Pleistocene marker from Angster et al. (2019) (Table 2). In the graph of Figure 11A, the oldest four offset geologic markers are plotted independently and are included with the offset normal fault and the late Pleistocene markers. Applying a Levenberg-Marquardt linear regression, which takes into account uncertainty in y- and x-values (Jolivette, 1993), through these six data points, yields an average long-term minimum dextral slip rate 0.4 ± 0.1 mm/yr since the paleovalley infilling unit Obmg was emplaced at 27.28 ± 0.02 Ma. In the graph of Figure 11B, the average offset of the four oldest geologic markers is plotted, along with the offset normal fault and the late Pleistocene markers. Applying a Levenberg-Marquardt linear regression through these three data points yields a long-term average slip rate of 0.5 ± 0.1 mm/yr since fault slip initiated between 15.99 ± 0.05 Ma and 15.71 ± 0.03 Ma. In this analysis, we assume that slip along the normal fault marker initiated at ca. 11.8 Ma, and slip along the Petrified Spring fault was continuous. If we assume a younger initiation age for the normal fault, for example 9.0 ± 0.1 Ma, then the calculated long-term average slip rate along the Petrified Spring fault is 0.6 ± 0.1 mm/yr (Fig. 11B). Another alternative slip history along the Petrified Spring fault might consist of three intervals, an initial rapid, maximum slip rate of 1.5 ± 0.5 mm/yr averaged between ca. 16.0 Ma and ca. 11.8 Ma during the first interval, a second, slower, minimum slip rate of 0.3 ± 0.2 mm/yr averaged between ca. 11.8 and ca. 124 ka (Fig. 11B), and a third slip rate of 0.7 +0.3/-0.2 mm/yr since ca. 124 ka (Angster et al., 2019).

Benton Spring Fault

Based on our detailed mapping along the southern 60% of the Benton Spring fault exposed in the Gabbs Valley Range, we identified four Cenozoic markers dextrally offset between ~5 km and ~9 km across this fault (Fig. 3).

The oldest marker dextrally offset by the Benton Spring fault is the same paleovalley incised into Mesozoic basement and infilled with unit Obmg that we mapped across the Petrified Spring fault (maroon marker in Fig. 3). Along the southern part of the Benton Spring fault, the southern paleovalley wall is well exposed on both sides of the fault and is developed in Mesozoic granite. At the contact, a paleosol, characterized by heavily fractured granite grading upwards into granite corestones surrounded by grus (Fig. 5A) to only grus, separates the underlying granite from the overlying Obmg. The northern paleovalley wall has been covered by younger Cenozoic tuffs. The southern paleovalley wall, which varies from a steep to shallow north dip, can be traced up to the fault on the west side, whereas it is projected ~300 m to the fault on the east side; thus we assign a 20% error to our dextral offset measurement of 7.2 ± 1.4 km (Fig. 3; Table 2).

Unit Osp (dark-blue marker in Fig. 3) defines the second marker dextrally offset across the Benton Spring fault. On both sides of the fault, unit Osp

Downloaded from http://pubs.geoscienceworld.org/gsa/geosphere/article-pdf/16/5/1249/5148564/1249.pdf
by University of Nevada Reno user

appears to be infilling a paleovalley inset into the older Benton Spring Group tuffs. On the east side of the fault, the southern contact between Osp and the paleovalley defining Benton Spring Group tuffs varies from shallow to steeply dipping (Figs. 3 and 5D), suggesting that the Osp here infilled the paleovalley before overflowing onto an adjacent floodplain. The northern contact is buried by younger volcanic units. On the west side of the fault, much of the southern contact is buried by younger volcanic units, and the northern contact with unit Obsi, into which the paleovalley incised, is typically near vertical. Assuming an EW-strike along the southern paleovalley contact on the west side of the fault, we measure 4.9 ± 2.5 km of dextral offset of this contact (Fig. 3; Table 2).

Unit Mrc (red marker in Fig. 3) is the third marker dextrally offset across the Benton Spring fault. On the east side of the Benton Spring fault, unit Mrc appears to infill two paleovalleys separated by ~2 km (Fig. 3). The southern paleovalley was inset into older lavas and tuffs. The southern contact between the infilling Mrc and paleovalley bedrock is shallowly dipping, whereas the northern contact is buried by the younger Mlf. The northern paleovalley was inset into units OMl and older tuffs in unit OMts. The map trace of this paleovalley's southern contact, between the infilling Mrc and the OMl-defined paleovalley wall, is NE-SW and steep to moderately north-dipping. The northern contact of this paleovalley is partially buried by the younger unit Mlf and, where exposed, exhibits a shallow contact with unit OMts. The latter contact geometry suggests that Mrc overflowed onto an adjacent floodplain. In contrast, on the west side of the Benton Spring fault, a single, well-exposed paleovalley infilled with unit Mrc is exposed in Wildhorse Canyon (Figs. 3, 8, and 9). The eastern extent of this part of the paleovalley is buried by Quaternary deposits and is projected ~750 m to the Benton Spring fault, whereas the western end of this paleovalley nearly abuts the Gumdrop Hills fault (Figs. 3 and 8). Restoring the southern walls of two Mrc infilled paleovalleys on the east side of the Benton Spring fault with the southern wall of the Wildhorse Canyon paleovalley yields dextral offset magnitudes of 12.6 ± 6.3 km (southern paleovalley) and 9.1 ± 2.7 km (northern paleovalley). We suggest that the northern paleovalley infilled with unit Mrc on the east side of the Benton Springs fault correlates to the Wildhorse Canyon paleovalley because the southern paleovalley walls on both sides of the fault record a NE-SW map trace and moderate to steep north dips. If our interpretation is correct, the dextral offset is 9.1 ± 2.7 km across this part of the Benton Spring fault (Fig. 3; Table 2).

The Rhyolite of Gabbs Valley Range (unit Mrl) defines a fourth dextrally offset geologic marker (dark-green marker in Fig. 3). On the east side of the Benton Spring fault, unit Mrl is moderately to poorly exposed and was emplaced in a paleovalley developed in older tuffs, lavas, and sediments (units OMts and Mrc) (Fig. 3). On the west side of the fault, the poorly exposed Mrl is inset into older tuffs and lavas (units Obsi, Osp, and OMl) and projected eastward ~2 km to the fault. Assuming the trend of our projection is correct, then Mrl is dextrally offset 6.7 ± 2.7 km across the Benton Spring fault (Fig. 3; Table 2).

Across the Benton Spring fault, the four markers—the ca. 27.1 Ma Obmg, the ca. 24.3 Ma Osp, the ca. 23.0 Ma Mrc, and the ca. 20.1 Ma unit Mrl—are dextrally offset 7.2 ± 1.4 km, 4.9 ± 2.5 km, 9.1 ± 2.7 km, and 6.7 ± 3.3 km, respectively.

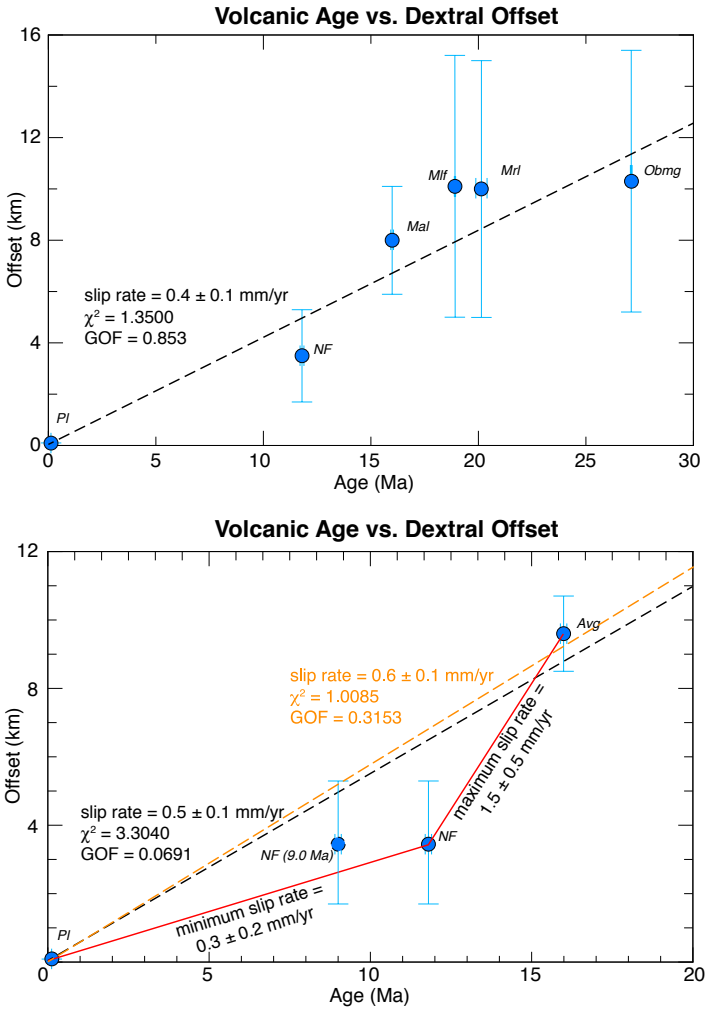

Figure 11. Plots of volcanic marker age versus dextral offset across the Petrified Spring fault. In (A), the four oldest markers (units Obmg, Mrl, Mlf, and Mal) are treated as separate data points implying that slip initiated after ca. 27.1 Ma; and in (B), the average (Avg) of the four oldest markers is plotted, implying that slip initiated after ca. 16.0 Ma (see Table 2). Applying a Levenberg-Marquardt regression (dashed black line) through data in (A) yields an average dextral slip rate of 0.4 ± 0.1 mm/yr since the late Oligocene and in (B) an average dextral slip rate of 0.5 ± 0.1 mm/yr since the middle Miocene. Dashed orange line in (B) shows an average dextral rate of 0.6 ± 0.1 mm/yr and is based on the assumption that slip along the normal fault marker occurred at 9.0 ± 0.1 Ma (see text for discussion). Solid red lines in (B) show a possible two-interval slip history since the middle Miocene. Uncertainty in offset and age are indicated by lines through data points, although nearly all data points are larger than the uncertainty associated with age values. Abbreviations: GOF—goodness of fit; NF—normal fault marker; Pl—late Pleistocene marker (Angster et al., 2019); unit labels defined in Figures 3 and 4.

Downloaded from http://pubs.geoscienceworld.org/gsa/geosphere/article-pdf/16/5/1249/5148564/1249.pdf
by University of Nevada Reno user

These measured offsets are the same, within error, and as a result, we interpret the average dextral offset of 7.0 ± 1.7 km as the best estimate for the maximum offset across the Benton Spring fault (Table 2). If our interpretation is correct, then slip along the Benton Spring fault initiated sometime after 20.14 ± 0.26 Ma, the age of the youngest offset unit (Mrl) and records a minimum average dextral slip rate of 0.4 ± 0.1 mm/yr since the early Miocene. If slip along the Benton Spring initiated at the same time as along the Petrified Spring fault, between 15.99 ± 0.05 Ma and 15.71 ± 0.03 Ma, then the long-term fault-slip rate is between 0.4 ± 0.1 mm/yr and 0.5 ± 0.1 mm/yr (Table 2).

Gumdrop Hills Fault

Along the Gumdrop Hills fault, we identified three tuff-filled paleovalleys—one infilled with unit Obmg (maroon marker), one infilled with unit Osp (dark-blue marker), and the last infilled with unit Mrc (red marker)—that record Cenozoic dextral offset (Fig. 3). On the east side of the southern Gumdrop Hills fault, the southern paleovalley wall between Mesozoic basement and the infilling Obmg is well exposed and can be traced farther east where it is dextrally offset by the Benton Spring and Petrified Spring faults. In contrast, the Obmg-infilled paleovalley on the west side of the Gumdrop Hills fault is poorly exposed. Thus, we assign a 50% error to our estimate of dextral offset of 4.6 ± 2.3 km for this paleovalley (Fig. 3; Table 2).

The Osp-infilled paleovalley is poorly exposed on both sides of the Gumdrop Hills fault, although locally near-vertical contacts implying steep paleovalley walls are present; thus we assign a 50% error to the estimated dextral offset of 9.7 ± 4.9 km (Fig. 3; Table 2).

On the east side of the Gumdrop Hills fault, the Wildhorse Canyon paleovalley infilled with Mrc (Figs. 3, 8, and 9) nearly abuts the fault. In sharp contrast, on the west side of the Gumdrop Hills fault in Nugent Wash, the Wildhorse Canyon paleovalley is preserved only as a few small outcrops of the infilling unit Mrc surrounded by Pliocene–Quaternary alluvial deposits (Fig. 3). Measuring the distance between the intersections of the Gumdrop Hills fault with the north and south paleovalley walls in Wildhorse Canyon and with their inferred counterparts straddling Nugent Wash yields dextral offset estimates of 10.7 ± 5.4 km and 8.8 ± 4.4 km (north and south paleovalley walls, respectively), or an average of 9.8 ± 1.3 km, since emplacement of unit Mrc at 22.95 ± 0.04 Ma (this study) (Fig. 3; Table 2).

Across the Gumdrop Hills fault, the magnitude of dextral offset increases from ~4.9 km in the southern part to 9.8 ± 1.3 km along the central part of the fault. If our interpretation is correct that slip along the Radio Tower fault is transferred to the central Gumdrop Hills fault, then this interpretation only partially explains the difference in slip magnitude between the southern and northern parts of the Gumdrop Hills fault. The two northern dextral offset measurements, 9.7 ± 4.9 km for the Osp infilled paleovalley and 9.8 ± 1.3 for the Mrc infilled paleovalley, are the same, within error. We, therefore, argue that the average dextral offset of 9.7 ± 1.0 km is the best estimate for the maximum offset across the Gumdrop Hills fault (Table 2). Slip initiated along the Gumdrop Hills fault sometime after emplacement of unit Mrc at 22.95 ± 0.04 Ma, thus indicating a long-term minimum dextral fault-slip rate of ~0.4 mm/yr. If slip initiated at the same time as along the Petrified Spring fault, then the long-term dextral slip rate is 0.6 ± 0.1 mm/yr (Table 2).

Radio Tower and Indian Head Faults

The Radio Tower and Indian Head faults cut Mesozoic sedimentary and intrusive rocks and Cenozoic volcanic rocks, although we did not observe any dextrally offset Cenozoic volcanic markers. However, we identified two near-vertical Mesozoic intrusive contacts as offset markers that strike approximately perpendicular to the faults. Along the Radio Tower fault, an intrusive contact between Jurassic sedimentary rocks and a Jurassic granodiorite records a dextral offset magnitude of 500 ± 50 m, and along the Indian Head fault an intrusive contact between the Triassic Luning Formation and a Jurassic diorite records a dextral offset magnitude of 5.0 ± 0.5 km (Table 2).

Neither fault can be traced northward into Win Wan Flat or Win Wan Valley, although Ekren and Byers (1985b) inferred that the map trace of the Indian Head fault continued to the northwest in Win Wan Valley where it was buried under Quaternary deposits (Fig. 3). To assess whether these faults might continue northward, we use the geologic maps of Ekren and Byers (1985b), Hardyman (1980), and Stewart et al. (1981) to interpret the location of the Obmg-infilled paleovalley in the western Gabbs Valley Range and the Gilles Range and to assess whether this paleovalley had been dextrally offset by the inferred buried faults (Fig. 3).

Our interpretation of these maps shows that the Obmg-infilled paleovalley meanders westward from the Gumdrop Hills fault across Win Wan Flat, Win Wan Valley, and Buckley Flat and does not require dextral offset across the inferred northward-projected traces of the Indian Head and Radio Tower faults (Fig. 3). Thus, dextral slip along the Radio Tower and Indian Head faults decreases and dies northward beyond their mapped trace. Our interpretation that slip along the Radio Tower fault is transferred northward onto the Gumdrop Hills fault provides a partial explanation for the apparent northward increase in dextral offset we observed along the Gumdrop Hills fault from ~4.9 km across the southern part of the fault to ~9.7 km in the central part. We also suggest that the slip along the Indian Head fault is transferred westward to the Agai Pah Hills fault across a contractional stepover. The most extensive exposures of Mesozoic bedrock in the GVGR are located in the proposed contractional stepover, and their exposure may be explained by contractional deformation and erosion.

Agai Pah Hills Fault

We did not map along the Agai Pah Hills fault; thus to extend paleovalleys westward across the Gillis Range, we reinterpret Hardyman's (1980) and Stewart

Downloaded from http://pubs.geoscienceworld.org/gsa/geosphere/article-pdf/16/5/1249/5148564/1249.pdf
by University of Nevada Reno user

et al.'s (1981) geologic maps of the region to show the locations of Obmg and Osp infilled paleovalleys and to document their dextral offsets. If our inferred westward trace of the southern wall of the Obmg paleovalley across Buckley Flat is correct (maroon marker in Fig. 3), then this paleovalley intersects and is dextrally offset by two strands of the southern Agai Pah Hills fault. Exposed on the west side of this fault are two east-west–trending swaths of unit Obmg straddling Mesozoic bedrock (Hardyman, 1980) (Fig. 3). The southern swath exposes moderate to steep contacts between unit Obmg and the underlying Mesozoic sediments, which we interpret as a paleovalley wall that defines a relatively narrow, 1.3-km-wide paleovalley. In contrast, the northern swath is characterized by shallow contacts between Mesozoic sedimentary and intrusive rocks and the overlying unit Obmg. We interpret these field relations as recording the deposition of Obmg upon a floodplain developed in Mesozoic bedrock. Alternatively, the two swaths of Obmg define a wide channel inset into a Mesozoic bedrock-defined interfluve. Using the southern paleovalley wall as a marker indicates 4.1 ± 2.1 km of dextral offset across the Agai Pah Hills fault (Fig. 3; Table 2).

The Osp-infilled paleovalley (dark-blue marker in Fig. 3) is more poorly exposed between the Gumdrop Hills fault and Agai Pah Hills fault compared to the Obmg-infilled paleovalley (Fig. 3). Our inferred trace of the southern Osp paleovalley wall across Buckley Flat indicates that this paleovalley intersects and is dextrally offset across two strands of the southern Agai Pah Hills fault (Fig. 3). Most of the southern Osp paleovalley wall on the west side of the fault has been eroded away; thus we assign a 50% error to the summed dextral offset of 5.6 ± 2.3 km (Fig. 3; Table 2).

The Obmg- and Osp-infilled paleovalleys are dextrally offset across the Agai Pah Hills fault by 4.1 ± 2.1 km and 5.6 ± 2.3 km, respectively. These measurements are the same, within error, yielding an average dextral offset across the Agai Pah Hills fault of 4.9 ± 1.1 km, indicating a minimum long-term dextral slip rate of 0.2 ± 0.1 mm/yr since emplacement of unit Osp at 24.30 ± 0.05 Ma. If slip initiated at the same time as along the Petrified Spring fault, then the long-term dextral slip rate is 0.3 ± 0.1 mm/yr (Table 2).

Cumulative Dextral Offset across the Gabbs Valley–Gillis Ranges

Of the five volcanic-filled paleovalleys exposed in the Gabbs Valley–Gillis Ranges, the Obmg-infilled paleovalley is the only marker that is offset across each of the four major faults—the Petrified Spring, the Benton Spring, the Gumdrop Hills, and Agai Pah Hills (Fig. 3). Thus, we can use this marker to calculate a cumulative dextral offset and average slip rate across the GVGR. Summing the calculated average dextral offsets for each of these faults, 9.6 ± 1.1, 7.0 ± 1.7, 9.7 ± 0.1, and 4.9 ± 1.1, respectively, yields a cumulative dextral offset of 31.2 ± 2.3 km. Our ~31.2 km estimate falls between the minimum and maximum estimates for cumulative offset, 26 and 60 km, of earlier work (Ekren et al., 1980; Ekren and Byers, 1984; Hardyman and Oldow, 1991; Oldow, 1992; Hardyman et al., 2000). Using our cumulative offset magnitude indicates that the minimum long-term dextral fault-slip rate across the GVGR is 1.2 ± 0.1 mm/yr since the emplacement of unit Obmg at ca. 27.1 Ma. If we assume that the initiation age for dextral fault slip on all faults is the same as documented for the Petrified Spring fault, between 15.99 ± 0.05 Ma and 15.71 ± 0.03 Ma, then the calculated geologic dextral slip rate across the GVGR is 2.0 ± 0.1/ ± 0.2 mm/yr. If our inference is incorrect that the slip along the Radio Tower and Indian Head faults is not transferred to the Gumdrop Hills and the Agai Pah Hills faults, respectively, then including the magnitude of offset along these two faults increases the cumulative dextral offset to 36.7 ± 2.6 km across the GVGR.

An obvious follow-on question is: can the Obmg-infilled paleovalley be traced westward from the western flank of the Gillis Range across the Walker Lake basin and into the Wassuk Range (Fig. 3)? Regional geologic relations suggest that the answer to this question is yes. However, due to the lack of exposed bedrock and faults in the Walker Lake basin, and limited exposure of unit Obmg in the Wassuk Range (Fig. 3), our estimated magnitude of dextral offset of the Obmg-infilled paleovalley across the Walker Lake basin is somewhat speculative. Although Obmg is not extensively exposed in the Wassuk Range, Bingler (1978) and Dilles (1992) noted that where mapped, Obmg-infilled topographic lows or valleys developed within the Mesozoic basement, which we suggest indicates Obmg-infilled paleovalleys (Fig. 3). Evidence for dextral slip between the western Gillis Range and the core of the Wassuk Range includes NW-striking dextral faults mapped within the Wassuk Range (Bingler, 1978; McIntyre, 1990), along the northeastern Wassuk range front (Dilles, 1992) and cutting late Pleistocene Lake Lahontan shorelines (Dong et al., 2014) (Fig. 3). Seismic data across Walker Lake showed NE-striking faults of unknown type and did not reveal NW-striking dextral faults in the subsurface (Dong et al., 2014). Given these limited data, and the noted caveats, we cautiously suggest that the Obmg-infilled paleovalley may record ~10 km of dextral slip between the western Gillis Range and the core of the Wassuk Range (Fig. 3). If true, our analysis indicates that the Obmg-infilled paleovalley records a cumulative dextral offset of ~39–44 km between the east side of Petrified Spring fault and the Wassuk Range. If all this slip initiated between 15.99 ± 0.05 Ma and 15.71 ± 0.03 Ma, then the long-term slip rate across the eastern central Walker Lane is 2.6 ± 0.1 mm/yr.

Vertical Offset Estimates

Our field observations, combined with review of geologic maps by Hardyman (1980) and Ekren and Byers (1985b), do not indicate a significant magnitude of vertical offset on the Petrified Spring, Benton Spring, Gumdrop Hills, Indian Head, and Agai Pah Hills faults. Field observations and geologic map interpretations, including alternating fault-scarp face directions, sub-vertical fault planes, and linear fault traces across topography, suggest nearly pure strike-slip motion. Limited exposures of slickenlines on the main trace of these faults record plunges that range from 06° to 28° toward the southeast, also indicating dominantly strike-slip motion.

Downloaded from http://pubs.geoscienceworld.org/gsa/geosphere/article-pdf/16/5/1249/5148564/1249.pdf
by University of Nevada Reno user

DISCUSSION

Fault Kinematics in the Eastern Central Walker Lane

Our geologic mapping, measured dextral offsets of paleovalley walls, and geochronology investigations, combined with interpretation of published geologic maps, across the GVGR, Central Walker Lane are the first to provide (1) detailed measurements of dextrally offset pre-Quaternary Cenozoic markers across the Petrified Spring, Benton Spring, Gumdrop Hills, and Agai Pah Hills faults, and (2) tight age brackets for initiation of fault slip on the Petrified Spring fault and maximum ages for initiation of fault slip on the Benton Spring, Gumdrop Hills, and Agai Pah Hills faults. Dextral fault slip in the GVGR is concentrated on the longest of these faults, the Petrified Spring, Benton Spring, and Gumdrop Hills faults (Fig. 3), which record the same magnitude of dextral offset, within error, at 9.6 ± 1.1 km, 7.0 ± 1.7 km, and 9.7 ± 1.0 km, respectively. The shorter Indian Head and Agai Pah Hills faults (Fig. 3) record dextral offset magnitudes of 5.0 ± 0.5 km and 4.9 ± 1.1 km, respectively, approximately half as much dextral offset as the longest faults. The shortest fault we mapped, the Radio Tower fault, records 0.5 ± 0.1 km of dextral offset of a Mesozoic marker. We suggest that slip along the Radio Tower fault is transferred northward onto the Gumdrop Hills fault. We interpret the left-stepping stepover geometry between the Indian Head and Agai Pah Hills faults as defining a contractional stepover in a dextral fault system (Fig. 3). We speculate that contractional deformation and erosion resulted in the extensive exposure of Mesozoic basement in the stepover region.

Initiation of fault slip along the Petrified Spring fault is tightly bracketed between 15.99 ± 0.05 Ma and 15.71 ± 0.03 Ma. For the other main faults—the Benton Spring, Gumdrop Hills, and Agai Pah Hills faults—we have only documented a maximum age for fault-slip initiation at 20.14 ± 0.26 Ma, 22.95 ± 0.04 Ma, and 24.30 ± 0.05 Ma, respectively. We do not have any age constraints for the onset of fault slip along the Radio Tower and Indian Head faults.

The Petrified Spring fault preserves evidence for progressive dextral offset whereby older offset geologic markers record a larger magnitude of offset. Thus, along this fault, slip rates may have changed with time, from initially a relatively fast rate to a slow rate and then to an intermediate rate (Fig. 11B). None of the other faults expose evidence for progressive offsets; thus, we cannot assess whether the GVGR region records a spatial-temporal distribution of fault slip.

Implications for Regional Fault Kinematics

The dextral faults in the GVGR are well exposed, but their along-strike continuation to the northwest and southeast is moderately to poorly constrained. To the northwest, the Petrified Spring fault appears to transition into an extensional right stepover defined by a set of NE-striking normal faults in the Gabbs Valley (Craig, 2019) (Figs. 2 and 3); these faults strike subparallel to NW-striking normal faults in western Basin and Range (Fig. 2). The northwest extent of the Benton Spring fault has been mapped along the northeast flank of the Terrill Mountains where it may record as much as ~6 km of dextral offset since ca. 23 Ma (Carlson, 2018). However, whether this fault can be traced northwestward to the eastern end of Carson domain, defined by clockwise-rotating blocks bounded by ENE-striking sinistral faults (e.g., Cashman and Fontaine, 2000) (Fig. 2), has not been documented. In addition, whether the Gumdrop Hills and Agai Pah Hills faults can be traced northwestward into or west of the Terrill Mountains is not known.

The Petrified Spring and Benton Spring faults extend to southeast and straddle the Pilot Mountains (Oldow and Meinwald, 1992; Oldow and Dockery, 1993) and perhaps continue farther south to straddle the Monte Cristo Range (Fig. 2). Here, these faults bound the eastern end of the Mina deflection, which like the Carson domain, is defined by clockwise-rotating blocks bounded by ENE-striking sinistral faults (e.g., DeLano et al., 2019; Petronis et al., 2019) (Fig. 2). The Indian Head fault may extend southward into Black Mountain (Fig. 2); it is not known whether the Gumdrop Hills and Agai Pah Hills faults can be traced south of Soda Spring Valley (Fig. 2).

Our geochronologic constraints on the initiation of dextral fault slip in the GVGR, bracketed between ca. 16.0 Ma and ca. 15.7 Ma, are similar to the predominantly ca. 18–12 Ma fault-slip initiation age along a number of range-bounding normal faults in the Walker Lane–northern Eastern California shear zone–western Basin and Range (for locations, see yellow stars in Fig. 2) (Table 3) and in eastern Nevada (e.g., Miller et al., 1999; Colgan et al., 2010). To the south of the GVGR field area, normal fault slip initiated at ca. 16 Ma along the east flank of the Inyo Mountains (Lee et al., 2009), at ca. 12 Ma along the west flank of the White Mountains (Stockli et al., 2003), and at ca. 18–12 Ma along the east-dipping Sierra Nevada frontal normal fault (Lee et al., 2020) (Fig. 2). To the northwest and west-northwest of the GVGR area, extension in the Yerington area and Singatse and Wassuk Ranges initiated at ca. 15–13 Ma (Dilles and Gans, 1995; Stockli et al., 2002; Surpless et al., 2002). Between the Wassuk Range to the north and White Mountains to the south is the Mina deflection (Fig. 2), a region that exposes normal faults with a palinspastically restored approximately north-south strike (restoration takes into account clockwise rotation of ~60° postfaulting; McCosby, 2019; Petronis et al., 2019) and a record of two phases of slip: (1) the first phase of fault slip, located in the eastern Queen Valley–Montgomery Pass area, predates ca. 12 Ma andesite (Tincher and Stockli, 2009); and (2) the second phase of fault slip, located in the Huntoon Mountains north of Queen Valley, is bracketed between ca. 12 Ma and ca. 3.8 Ma (McCosby, 2019). To the west of the Singatse and Wassuk Ranges, middle Miocene(?) normal faults are buried in the Gardnerville Basin (Cashman et al., 2009), and normal faulting initiated at ca. 12 Ma along the east-dipping Donner Pass fault zone located within the eastern margin of the Sierra Nevada southwest of Reno, Nevada (Henry and Perkins, 2001) (Fig. 2). To the northeast and east of the GVGR, range-bounding normal fault slip initiated at 20(?)–14 Ma along the Stillwater-East-Tobin ranges (Fosdick and Colgan, 2008; Gonsior and Dilles, 2008; MacNamee, 2015; Colgan et al., 2020), initiated at 17–15 Ma along the Toiyabe-Shoshone ranges (Stockli, 1999;

Downloaded from http://pubs.geoscienceworld.org/gsa/geosphere/article-pdf/16/5/1249/5148564/1249.pdf
by University of Nevada Reno user

TABLE 3. DOCUMENTED MIDDLE MIOCENE FAULT INITIATION AGE WITHIN THE WALKER LANE–NORTHERN EASTERN CALIFORNIA SHEAR ZONE–WESTERN BASIN AND RANGE

Range	Location number§	Initiation age (Ma)*	Reference
East Range	1	17–15	Fosdick and Colgan (2008)
Gardnerville Basin	2	Middle Miocene(?)	Cashman et al. (2009)
Gabbs Valley–Gillis Ranges (GVGR)	3	Ca. 16	This study
Inyo Mountains	4	Ca. 15	Lee et al. (2009)
Mina Deflection	5	>12 and ca. 12–3.8	Tincher and Stockli (2009); McCosby (2019)
Paradise Range	6	22–19†	John et al. (1989)
San Antonio Mountains	7	24.0–16.8†	Shaver and McWilliams (1987)
Shoshone and northern Toiyabe Ranges	8	17–16	Colgan et al. (2008)
Southern Sierra Nevada	9	Ca. 18–12	Lee et al. (2020)
Singatse Range	10	Ca. 15–13	Dilles and Gans (1995); Surpless et al. (2002); Stockli et al. (2002)
Southern Stillwater Range	11	18–14	Colgan et al. (2020)
Northern Stillwater Range	12	Ca. 14	MacNamee (2015)
Tobin Range	13	20(?)–14	Gonsior and Dilles (2008)
Toiyabe Range	14	Ca. 15	Stockli (1999)
Verdi Basin	15	Ca. 12	Henry and Perkins (2001)
Wassuk Range	16	Ca. 15	Surpless et al. (2002)
Northern White Mountains	17	Ca. 12	Stockli et al. (2003)

§For location of study areas, see numbered yellow stars in text Figure 2.
*Unless otherwise indicated, age constraints are from low-temperature thermochronology studies of footwall rocks and/or $^{40}Ar/^{39}Ar$ geochronology on offset volcanic rocks.
†K/Ar geochronology on offset volcanic rocks.

Colgan et al., 2008), and ca. 24–17 Ma along the western flank of the Paradise and San Antonio ranges (Shaver and McWilliams, 1987; John et al., 1989).

In contrast to the growing database of middle Miocene age for initiation of faulting throughout the Walker Lane–northern Eastern California shear zone–Basin and Range region, there is scant evidence for Oligocene to early Miocene fault slip. In the northern Wassuk Range, a combination of geologic mapping and $^{40}Ar/^{39}Ar$ geochronology shows that slip along NW-striking dextral and normal faults initiated at ca. 27–25 Ma (Dilles and Gans, 1995), ~10 m.y. earlier than elsewhere in this region, and was ongoing at 23–22 Ma, thus defining a narrow zone of faulting that Dilles and Gans (1995) referred to as the Ancestral Walker Lane. In the Tobin Range, geologic mapping and $^{40}Ar/^{39}Ar$ geochronology data indicate a minor phase of normal faulting that initiated in the early Oligocene (Gonsior and Dilles, 2008). To our knowledge, fault slip of Oligocene to early Miocene age has not been documented anywhere else across the Walker Lane–northern Eastern California shear zone–western Basin and Range region, implying that the Oligocene to early Miocene-age faulting was restricted to small, local areas. In support of the absence of regional Oligocene to early Miocene faulting are observations that tuffs as young as ca. 23 Ma flowed in paleovalleys westward from central Nevada across what is now the western Basin and Range and Sierra Nevada into the Great Valley, implying a lack of topographic relief that could have disturbed westward-flowing paleovalleys (Henry et al., 2012).

Dilles and Gans (1995) also documented that the dextral and normal faults in the northern Wassuk Range were active again during the middle Miocene. Thus, during the middle Miocene, the dextral faults in the GVGR and in the northern Wassuk Range defined a NW-striking, left-stepping en echelon array of strike-slip faults, suggesting an areally more extensive Ancestral Walker Lane than originally envisioned by Dilles and Gans (1995) and the oldest dextral faults within the Walker Lane–eastern California shear zone (cf. Reheis and Sawyer, 1997; Stockli et al., 2003; Faulds and Henry, 2008 and references therein; this study).

Given the (1) similarity in initiation age between dextral faulting in the GVGR and normal faulting throughout the central Walker Lane–northern Eastern California shear zone–western Basin and Range region and (2) location of the GVGR between NE-striking normal faults in the western Great Basin to the north and NNW-striking normal faults in the northern Eastern California shear zone to the south (Fig. 2), we hypothesize that the NW-striking dextral faults in the GVGR defined a middle Miocene kinematic link or accommodation zone (e.g., Chapin et al., 1978; Faulds et al., 1990) between two regions that record different extension directions—NW-SE extension in the western Basin and Range and ENE-WSW extension in the northern Eastern California shear zone (Fig. 2).

Origin of NW-Dextral Faulting in the Ancestral Walker Lane

Our kinematic link or accommodation zone hypothesis above builds upon a postulate of Dilles and Gans (1995) whereby the Ancestral Walker Lane defined a transtensional accommodation zone separating extension in the western

Downloaded from http://pubs.geoscienceworld.org/gsa/geosphere/article-pdf/16/5/1249/5148564/1249.pdf
by University of Nevada Reno user

Basin and Range to the east from the Sierra Nevada block to the west. However, we now know that middle Miocene extension was also ongoing to the west in the Walker Lane–northern Eastern California shear zone (Fig. 2; Table 3). Dilles and Gans (1995) also proposed that development of dextral faults in the Ancestral Walker Lane was in response to dextral slip along the San Andreas fault. However, the link between onset of dextral fault slip in the Ancestral Walker Lane to slip along the San Andreas fault seems unlikely because the Mendocino Triple Junction was well south of the GVGR–northern Wassuk Range area during the late Oligocene to middle Miocene (DeMets and Merkouriev, 2016) (Fig. 12). Based on Pacific–North American plate reconstructions, the Mendocino Triple Junction did not reach the latitude of the GVGR–northern Wassuk Range area until early Pliocene (DeMets and Merkouriev, 2016) (Fig. 12), thus raising the question: What drove initiation of dextral slip in the Central Walker Lane? We address this question below.

The NW-striking dextral faults exposed within the GVGR are part of the eastern California shear zone–Walker Lane dextral shear zone that today accommodates ~20%–25% of Pacific–North America plate motion (e.g., Thatcher et al., 1999; Dixon et al., 2000; Bennett et al., 2003; Lifton et al., 2013; Bormann et al., 2016) (Fig. 1). The azimuth of GPS vectors, relative to the North American plate, in the GVGR area is nearly parallel to the motion of the SN-CGB (cf. Bennett et al., 2003; Lifton et al., 2013; Bormann et al., 2016) (Fig. 2). Thus, dextral motion across the Pacific–North America plate boundary is the primary driver for dextral fault slip today across the GVGR. However, if dextral fault slip in the GVGR initiated during the middle Miocene and defines an accommodation zone between regions of NW-SE and NNE-SSW extension, the plate tectonic setting along the western margin of the North America plate at the latitude of the GVGR was not characterized by dextral shear.

Based on plate reconstructions during the middle Miocene, the GVGR and normal faults of similar age in the western Basin and Range and the northern Eastern California shear zone were located at least ~1.75° to ~3.75° of latitude north of the Mendocino Triple Junction and east of a plate boundary characterized by northeast (oblique) subduction of the Juan de Fuca plate beneath the North American plate (e.g., Engebretson et al., 1985; Gordon and Jurdy, 1986; Atwater and Stock, 1998; DeMets and Merkouriev, 2016) (Fig. 12). Crustal extension of the proto–Basin and Range has been explained by a combination of gravitational potential energy and plate boundary processes (e.g., Sonder and Jones, 1999; Dickinson, 2002; Colgan and Henry, 2009). Prior to the onset of middle Miocene extension, the proto–Basin and Range region was characterized by high gravitational potential energy, postulated to be a consequence of thickened crust and high elevations following Mesozoic contraction (e.g., DeCelles, 2004; Lechler et al., 2013) as well as hot, buoyant asthenosphere that had replaced the Farallon slab following its steepening and falling away (e.g., Armstrong and Ward, 1991; Humphreys, 1995; Humphreys, 2009; Schmandt and Humphreys, 2011) and the emplacement of the Yellowstone hotspot (e.g., Parsons et al., 1994; Saltus and Thompson, 1995). Trench retreat along the Juan de Fuca–North American plate subduction zone, combined with a Basin and Range primed for extension and stable North America acting as a lithostatic backstop, drove westward motion of the rigid Sierra Nevada–Great Valley block, and behind the block westward collapse and concomitant east-west extension of the Basin and Range (e.g., Dickinson, 2002; Colgan and Henry, 2009; McQuarrie and Oskin, 2010) (Fig. 12). Thus, the driving mechanism for onset of and the first ~10 m.y. of dextral slip across the GVGR, which defined a kinematic link between two zones of extension, was trench retreat superimposed on continental crust that was ready to extend.

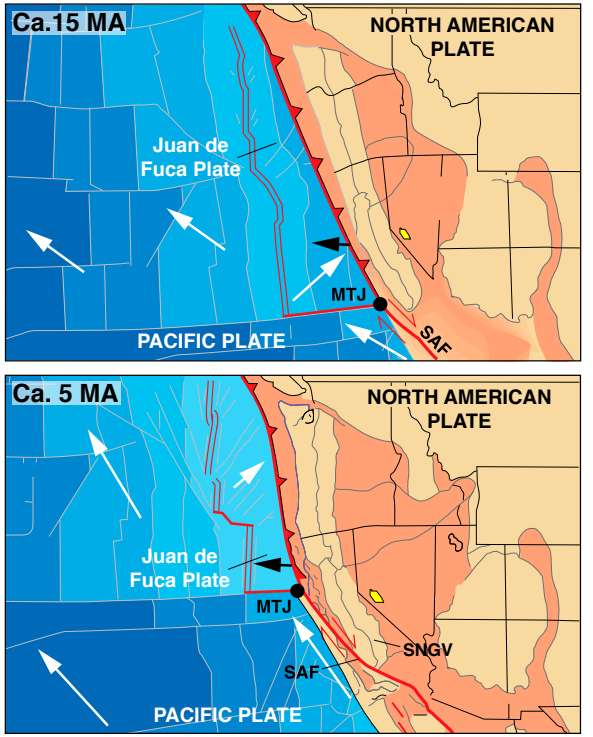

Figure 12. Maps showing location of the Gabbs Valley–Gilles Ranges field area (yellow polygon; see Fig. 3) in the context of a reconstruction of the Juan de Fuca–Pacific–North American plates at ca. 15 Ma and ca. 5 Ma. Double red lines define a mid-ocean ridge; heavy red lines define a fracture zone or a transform fault; heavy red lines with solid teeth define a subduction zone; light to dark blue colors indicate relative ages, from young to old, of oceanic crust; heavy white arrows on the Pacific and Juan de Fuca plates indicate motion of that plate with respect to a fixed North American plate; heavy black arrow schematically illustrates motion of the trench with respect to a fixed North American plate. Salmon color shows zones of deformation in the North American plate. MTJ—Mendocino triple junction; SAF—San Andreas fault; SNGV—Sierra Nevada-Great Valley block. Maps are modified from Faulds and Henry (2008), which were modified from Atwater (http://emvc.geol.ucsb.edu/1_DownloadPage/Download_Page.html) and include an interpolation of position of the MTJ based on reconstructions in DeMets and Merkouriev (2016).

Downloaded from http://pubs.geoscienceworld.org/gsa/geosphere/article-pdf/16/5/1249/5148564/1249.pdf
by University of Nevada Reno user

Plate reconstructions show that since the early Pliocene, the Mendocino Triple Junction has been located at the same latitude as or north of the GVGR (DeMets and Merkouriev, 2016) (Fig. 12); thus, during the past ~5 m.y. history of dextral slip across the GVGR, the plate boundary setting had changed to a transform boundary. The sum of Pliocene and younger fault-slip rates across the northern Eastern California shear zone show that dextral fault slip accounts for ~20%–25% of Pacific–North America plate transform motion (e.g., Frankel et al., 2007; Lee et al., 2009; DeLano et al., 2019; Lifton et al., 2020). Thus, since the Pliocene, dextral transform slip along the San Andreas fault characterized the Pacific–North American plate boundary west of the northern Eastern California shear zone–Central Walker Lane region, and that plate boundary shear continued to drive dextral slip in the GVGR. This kinematic geometry implies that the sub-parallelism between motion of the SN-CGB and strike of the main dextral faults in the GVGR at ~323° is coincidental, but ideal for reactivation.

CONCLUSIONS

Our new geologic mapping, structural, and geochronologic data across the GVGR region, combined with published geologic maps, and active tectonic and GPS studies of the GVGR region, reveal histories of late Oligocene to Pliocene volcanism-magmatism and middle Miocene to present-day deformation across an ~35-km-wide zone characterized by NW-dextral slip distributed along four primary faults—the Petrified Spring, Benton Spring, Gumdrop Hills, and Agai Pah Hills–Indian Head faults. Based on data from our investigations, we document dextrally offset pre-Quaternary Cenozoic tuff- and lava-filled paleovalleys and other markers across the faults, we calculate new dextral fault-slip rates along each fault, and we calculate a cumulative fault offset magnitude and fault-slip rate across the GVGR. Our measured dextral offset across the Petrified Spring, Benton Spring, and Gumdrop Hills faults ranges from ~9.7–7.0 km, and across the Agai Pah Hills–Indian Head fault is ~5.0 km. Dextral slip initiated post–late Oligocene to middle Miocene; our preferred interpretation is that dextral slip initiated between ca. 15.99 Ma and ca. 15.71 Ma, the tight age bounds for onset of slip along the Petrified Spring fault. Dextral slip rates on individual faults range from ~0.6 mm/yr to ~0.3 mm/yr. Progressive offsets across the Petrified Spring fault suggest a slip rate that varies with time is a permissible interpretation. Thus, this fault may record a finite strain history that is episodic. The absence of progressive offsets along the other dextral faults precludes assessing whether the eastern Central Walker Lane fault-slip history is characterized by episodic or non-episodic strain. The cumulative dextral offset and slip rate across the GVGR is measured at ~31.2 km and calculated at ~2.0 mm/yr.

Middle Miocene initiation of dextral fault slip in the GVGR overlaps with the timing of onset of fault slip on range-bounding normal faults across the Basin and Range Province, including the adjacent western Basin and Range to the north and the northern Eastern California shear zone to the south. We propose that the dextral faults of the GVGR define a kinematic link or accommodation zone between the northeast-striking normal faults in the western Basin and Range and the north-northwest–striking normal faults in the northern Eastern California shear zone. To our knowledge, there are no other faults in the Walker Lane–Eastern California shear zone that record dextral slip of middle Miocene age.

The plate tectonic setting along the western margin of the North American continent west of the GVGR changed during the ca. 16 Ma long history of dextral slip. During the middle Miocene, the GVGR was located north of the Mendocino Triple Junction, thus dextral fault slip could not have been driven by dextral shear along the Pacific–North American plate boundary. We postulate that the onset of dextral slip in the GVGR accommodation zone was driven by trench retreat along the Farallon plate–North American plate subduction zone into east-west extension across the proto–Basin and Range, which was primed for extension. With the arrival of the Mendocino Triple Junction at the same latitude as the GVGR, dextral fault slip was driven by dextral shear along the Pacific–North American plate boundary and was accommodated on the same set of faults that were fortuitously subparallel to SN-CGB motion. Because slip along the dextral faults in the GVGR were driven by changing plate tectonic settings, the long-term (10^6 yr) average geologic slip rates we estimate for the faults in the GVGR cannot be correlated to short-term (10^3–10^4 yr) or present-day (10^1 yr) slip rates, which accrued during a single plate tectonic setting.

ACKNOWLEDGMENTS

Thanks to Drew Abts and Zac Bales for their exceptional assistance with field work. Field discussions with Joe Colgan, Chris Henry, David John, and Sarah Nagorsen were invaluable. We benefitted from thoughtful discussions with Jackie Langille, Kim Blisniuk, and Warren Sharpe on the active faulting history in the GVGR, with Joann Stock about plate motions, with Zack Lifton and James Dolan about GPS versus geologic slip rates, with Chris Henry about western Basin and Range volcanism and extension, and with John Dilles about the geology in the northern Wassuk Range. Thanks to Dean Miller, James Saburomaru, and Katie Sullivan at the U.S. Geological Survey in Menlo Park for their help with sample separation and irradiation preparations. Special thanks to Walter Szeliga for his help processing GPS data. Informative and constructive comments from reviewers Chad Carlson and Chris Henry, and Associate Editor Andrew Zuza improved the clarity of our data descriptions and interpretations. Primary funding for this project was provided by a National Science Foundation grant #EAR-1419808 and U.S. Geological Survey–National Cooperative Geologic Mapping Program grants, G17AC00197 and G15AC00171, awarded to J. Lee. Additional funding was provided by a Geological Society of America Graduate Student Research Grant, 11768-17, awarded to A. Hoxey. Stereonet plots were produced using Stereonet 9.9.3 software thanks to Rick Allmendinger. Thanks to Chris Henry for providing a shaded relief map of Nevada from which the area of Figure 2 was extracted. Any use of trade, firm, or product names is for descriptive purposes only and does not imply endorsement by the U.S. Government.

REFERENCES CITED

Angster, S.J., Wesnousky, S.G., Figueiredo, P.M., Owen, L.A., and Hammer, S.J., 2019, Late Quaternary slip rates for faults of the central Walker Lane (Nevada, USA): Spatiotemporal strain release in a strike-slip fault system: Geosphere, v. 15, p. 1460–1478, https://doi.org/10.1130/GES02088.1.

Armstrong, R.L. and Ward, P., 1991, Evolving geographic patterns of Cenozoic magmatism in the North American Cordillera: The temporal and spatial association of magmatism and metamorphic core complexes: Journal of Geophysical Research, v. 96, p. 13,201–13,224.

Downloaded from http://pubs.geoscienceworld.org/gsa/geosphere/article-pdf/16/5/1249/5148564/1249.pdf
by University of Nevada Reno user

Atwater, T., and Stock, J.M., 1998, Pacific–North America plate tectonics of the Neogene southwestern United States: An update: International Geology Review, v. 40, p. 375–402, https://doi.org/10.1080/00206819809465216.

Bell, J.W., dePolo, C.M., Ramelli, A.R., Sarna-Wojcicki, A.M., and Meyer, C.E., 1999, Surface faulting and paleoseismic history of the 1932 Cedar Mountain earthquake area, west-central Nevada, and implications for modern tectonics of the Walker Lane: Geological Society of America Bulletin, v. 111, p. 791–807, https://doi.org/10.1130/0016-7606(1999)111<0791:SFAPHO>2.3.CO;2.

Bennett, R.A., Wernicke, B.P., Niemi, N.A., Friedrich, A.M., and Davis, J.L., 2003, Contemporary strain rates in the northern Basin and Range province from GPS data: Tectonics, v. 22, https://doi.org/10.1029/2001TC001355.

Bingler, E.C., 1978, Geologic Map of Schurz Quadrangle: Nevada Bureau of Mines and Geology, Map 60, scale 1:48,000.

Bormann, J.M., Hammond, W.C., Kreemer, C., and Blewitt, G., 2016, Accommodation of missing shear strain in the Central Walker Lane, western North America: Constraints from dense GPS measurements: Earth and Planetary Science Letters, v. 440, p. 169–177, https://doi.org/10.1016/j.epsl.2016.01.015.

Carlson, C.W., 2018, Geologic map of the Terrill Mountains quadrangle, Churchill and Mineral counties, Nevada: Nevada Bureau of Mines and Geology Field Studies Map 187, scale 1:24,000.

Cashman, P.H., and Fontaine, S.A., 2000, Strain partitioning in the northern Walker Lane, western Nevada and northeastern California: Tectonophysics, v. 326, p. 111–130, https://doi.org/10.1016/S0040-1951(00)00149-9.

Cashman, P.H., Trexler, J.H., Jr., Muntean, T.W., Faulds, J.E., Louie, J.N., and Oppliger, G.L., 2009, Neogene tectonic evolution of the Sierra Nevada–Basin and Range transition zone at the latitude of Carson City, Nevada, *in* Oldow, J.S., and Cashman, P.H., eds., Late Cenozoic Structure and Evolution of the Great Basin–Sierra Nevada Transition: Geological Society of America Special Paper 447, p. 171–188, https://doi.org/10.1130/2009.2447(10).

Chapin, C.E., Chamberlin, R.M., Osburn, G.R., and White, D.L., and Sanford, A.R., 1978, Exploration framework of the Socorro geothermal area, Field guide to selected cauldrons and mining districts of the Datil-Mogollon volcanic field: New Mexico Geological Society Special Publication 7, p. 114–129.

Colgan, J.P., and Henry, C.D., 2009, Rapid middle Miocene collapse of the Mesozoic orogenic plateau in north-central Nevada: International Geology Review, v. 51, p. 920–961, https://doi.org/10.1080/00206810903056731.

Colgan, J.P., and Henry, C.D., 2017, Eruptive History, Geochronology, and Post-Eruption Structural Evolution of the Late Eocene Hall Creek Caldera, Toiyabe Range, Nevada: U.S. Geological Survey Professional Paper 1832, 43 p., https://doi.org/10.3133/pp1832.

Colgan, J.P., John, D.A., Henry, C.D., and Fleck, R.J., 2008, Large-magnitude Miocene extension of the Eocene Caetano caldera, Shoshone and Toiyabe Ranges, Nevada: Geosphere, v. 4, no. 1, p. 107–130, https://doi.org/10.1130/GES00115.1.

Colgan, J.P., Howard, K.A., Fleck, R.J., and Wooden, J.L., 2010, Rapid middle Miocene extension and unroofing of the southern Ruby Mountains, Nevada: Tectonics, v. 29, TC6022, https://doi.org/10.1029/2009TC002655.

Colgan, J.P., Johnstone, S.A., and Shuster, D.L., 2020, Timing of Cenozoic extension in the southern Stillwater Range and Dixie Valley, Nevada: Tectonics, v. 39, no. 3, e2019TC005757, https://doi.org/10.1029/2019TC005757.

Craig, J.W., 2019, Discovery and analysis of a blind geothermal system in the southeastern Gabbs Valley, western Nevada: Geological Society of America Abstracts with Programs, v. 51, paper 94-2, https://doi.org/10.1130/abs/2019AM-337585.

Cunningham, W.D., and Mann, P., 2007, Tectonics of strike-slip restraining and releasing bends, *in* Cunningham, W.D., and Mann, P., eds., Tectonics of Strike-Slip Restraining and Releasing Bends: Geological Society of London Special Publication 290, p. 1–12, https://doi.org/10.1144/SP290.1.

DeCelles, P.G., 2004, Late Jurassic to Eocene evolution of the Cordilleran thrust belt and foreland basin system, western USA: American Journal of Science, v. 304, p. 105–168, https://doi.org/10.2475/ajs.304.2.105.

DeLano, K., Lee, J., Roper, R., and Calvert, A., 2019, Dextral, normal, and sinistral faulting across the Eastern California shear zone–Mina deflection transition, California-Nevada: Geosphere, v. 15, no. 4, p. 1206–1239, https://doi.org/10.1130/GES01636.1.

DeMets, C., and Merkouriev, S., 2016, High-resolution reconstructions of Pacific–North American plate motion: 20 Ma to present: Geophysical Journal International, v. 207, p. 741–773, https://doi.org/10.1093/gji/ggw305.

Dickinson, W.R., 2002, The Basin and Range province as a composite extensional domain: International Geology Review, v. 44, p. 1–38, https://doi.org/10.2747/0020-6814.44.1.1.

Dilles, J.H., 1992, Cenozoic normal and strike-slip faults in the northern Wassuk Range, western Nevada, *in* Craig, S.D., ed., Structure, Tectonics, and Mineralization of the Walker Lane: Reno, Nevada, Walker Lane Symposium Proceedings, Geological Society of Nevada, p. 114–136.

Dilles, J.H., and Gans, P.B., 1995, The chronology of Cenozoic volcanism and deformation in the Yerington area, western Basin and Range and Walker Lane: Geological Society of America Bulletin, v. 107, p. 474–486, https://doi.org/10.1130/0016-7606(1995)107<0474:TCOCVA>2.3.CO;2.

Dixon, T.H., Robaudo, S., Lee, J., and Reheis, M.C., 1995, Constraints on present-day Basin and Range deformation from space geodesy: Tectonics, v. 14, p. 755–772, https://doi.org/10.1029/95TC00931.

Dixon, T.H., Miller, M., Farina, F., Wang, H., and Johnson, D., 2000, Present-day motion of the Sierra Nevada block and some tectonic implications for the Basin and Range province, North American Cordillera: Tectonics, v. 19, no. 1, p. 1–24, https://doi.org/10.1029/1998TC001088.

Dokka, R.K., and Travis, C.J., 1990, Role of the eastern California shear zone in accommodating Pacific-North American plate motion: Geophysical Research Letters, v. 17, https://doi.org/10.1029/GL017i009p01323.

Dong, S., Ucarkus, G., Wesnousky, S.G., Maloney, J., Kent, G., Driscoll, N., and Baskin, R., 2014, Strike-slip faulting along the Wassuk Range of the northern Walker Lane, Nevada: Geosphere, v. 10, p. 40–48, https://doi.org/10.1130/GES00912.1.

Eckberg, E.E., Hitzman, M., Manydeeds, S., and Nelson, E.P., 1995, Evidence for pre-Walker Lane extension in the Copper Hill area, NW Gillis Range, Mineral County, Nevada, *in* Rhoden, H.N., Steininger, R.C., and Vikre, P.G., eds., Geological Society of Nevada Symposium 2005: Reno, Nevada, Window to the World, May 2005, p. 315–326.

Ekren, E.B., and Byers, F.M., Jr., 1984, The Gabbs Valley Range–A well-exposed segment of the Walker Lane in west-central Nevada, *in* Lintz, J., Jr., ed., Western Geological Excursions Guidebook: Geological Society of America, p. 203–215.

Ekren, E.B., and Byers, F.M., Jr., 1985a, Geologic map of the Gabbs Mountain, Mount Ferguson, Luning, and Sunrise Flat Quadrangles, Mineral County, Nevada, U.S. Geological Survey, Miscellaneous Investigations Series, Map I-1577.

Ekren, E.B., and Byers, F.M., Jr., 1985b, Geologic map of the Win Wan Flat, Kinkaid NW, Kinkaid, and Indian Head Peak Quadrangles, Mineral County, Nevada: U.S. Geological Survey, Miscellaneous Investigations Series, Map I-1578.

Ekren, E.B., and Byers, F.M., Jr., 1986a, Geologic map of the Murphys Well, Pilot Cone, Copper Mountain, and Poinsettia Spring Quadrangles, Mineral County, Nevada: U.S. Geological Survey, Miscellaneous Investigations Series, Map I-1576.

Ekren, E.B., and Byers, F.M., Jr., 1986b, Geologic map of the Mount Annie NW, Mount Annie, Ramsay Spring, and Mount Annie SE Quadrangles, Mineral County, Nevada: U.S. Geological Survey, Miscellaneous Investigations Series, Map I-1579.

Ekren, E.B., Byers, F.M., Jr., Hardyman, R.F., Marvin, R.F., and Silberman, M.L., 1980, Stratigraphy, preliminary petrology, and some structural features of Tertiary volcanic rocks in the Gabbs Valley an Gillis Ranges, Mineral County, Nevada: U.S. Geological Survey Bulletin 1464, 54 p.

Engebretson, D.C., Cox, A., and Gordon, R.G., 1985, Relative Motions between Oceanic and Continental Plates in the Pacific Basin: Geological Society America Special Paper 206, 59 p., https://doi.org/10.1130/SPE206-p1.

Faulds, J.E., and Henry, C.D., 2008, Tectonic influences on the spatial and temporal evolution of the Walker Lane: An incipient transform fault along the evolving Pacific–North American plate boundary: Ores and Orogenesis: Circum-Pacific Tectonics, Geologic Evolution, and Ore Deposits: Arizona Geological Society Digest, v. 22, p. 437–470.

Faulds, J.E., Geissman, J.W., and Mawer, C.K., 1990, Structural development of a major extensional accommodation zone in the Basin and Range Province, northwestern Arizona and southern Nevada: Implications for kinematic models of continental extension, *in* Wernicke, B.P., ed., Basin and Range Extensional Tectonics near the Latitude of Las Vegas, Nevada: Geological Society of America Memoir 176, p. 37–76, https://doi.org/10.1130/MEM176-p37.

Fleck, R.J., Calvert, A.T., Coble, M.A., Wooden, J.L., Hodges, K., Hayden, L.A., van Soest, M.C., du Bray, E.A., and John, D.A., 2019, Characterization of the rhyolite of Bodie Hills and $^{40}Ar/^{39}Ar$ intercalibration with Ar mineral standards: Chemical Geology, v. 525, p. 282–302, https://doi.org/10.1016/j.chemgeo.2019.07.022.

Flesch, L.M., Holt, W.E., Haines, A.J., and Shen-Tu, B., 2000, Dynamics of the Pacific–North American plate boundary in the western United States: Science, v. 287, p. 834–836, https://doi.org/10.1126/science.287.5454.834.

Downloaded from http://pubs.geoscienceworld.org/gsa/geosphere/article-pdf/16/5/1249/5148564/1249.pdf
by University of Nevada Reno user

Fosdick, J.C., and Colgan, J.P., 2008, Miocene Extension in the East Range, Nevada: A Two-Stage History of Normal Faulting in the Northern Basin and Range: Geological Society of America Bulletin, v. 120, p. 1198–1213, https://doi.org/10.1130/B26201.1.

Frankel, K.L., Brantley, K.S., Dolan, J.F., Finkel, R.C., Klinger, R.E., Knott, J.R., Machette, M.N., Owen, L.A., Phillips, F.M., Slate, J.L., and Wernicke, B.P., 2007, Cosmogenic ^{10}Be and ^{36}Cl geochronology of offset alluvial fans along the northern Death Valley fault zone: Implications for transient strain in the eastern California shear zone: Journal of Geophysical Research, v. 112, B06407, https://doi.org/10.1029/2006JB004350.

Gonsior, Z.J., and Dilles, J.H., 2008, Timing and evolution of Cenozoic extensional normal faulting and magmatism in the southern Tobin Range, Nevada: Geosphere, v. 4, p. 687–712, https://doi.org/10.1130/GES00137.1.

Gordon, R.G., and Jurdy, D.M., 1986, Cenozoic global plate motions: Journal of Geophysical Research, v. 91, p. 12,389–12,406, https://doi.org/10.1029/JB091iB12p12389.

Hardyman, R.F., 1978, Volcanic stratigraphy and structural geology of Gillis Canyon Quadrangle, Northern Gillis Range, Mineral County, Nevada [Ph.D. thesis]: Reno, Nevada, University of Nevada, 377 p.

Hardyman, R.F., 1980, Geologic map of the Gillis Canyon Quadrangle, Mineral County, Nevada, U.S. Geological Survey, Miscellaneous Investigations Series, Map I-1237.

Hardyman, R.F., and Oldow, J.S., 1991, Tertiary tectonic framework and Cenozoic history of the central Walker Lane, Nevada, *in* Raines, G.L., Lisle, R.E., Schafer, R.W., and Wilkinson, W.H., eds., Geology and Ore Deposits of the Great Basin: Reno, Nevada, Geological Society of Nevada Symposium Proceedings, v. 1, p. 279–301.

Hardyman, R.F., Ekren, E.B., and John, D.A., 2000, Evidence for Cenozoic dextral displacement across the Walker Lane, west-central Nevada: Geological Society of America Abstracts with Programs, v. 32, p. 105.

Henry, C.D., and Faulds, J.E., 2010, Ash-flow tuffs in the Nine Hill, Nevada, paleovalley and implications for tectonism and volcanism of the western Great Basin, USA: Geosphere, v. 6, p. 339–369, https://doi.org/10.1130/GES00548.1.

Henry, C.D., and John, D.A., 2013, Magmatism, ash-flow tuffs, and calderas of the ignimbrite flareup in the western Nevada volcanic field, Great Basin, USA: Geosphere, v. 9, no. 4, p. 951–1008, https://doi.org/10.1130/GES00867.1.

Henry, C.D., and Perkins, M.E., 2001, Sierra Nevada–Basin and Range transition near Reno, Nevada: Two-stage development at 12 and 3 Ma: Geology, v. 29, p. 719–722, https://doi.org/10.1130/0091-7613(2001)029<0719:SNBART>2.0.CO;2.

Henry, C.D., Hinz, N.H., Faulds, J.E., Colgan, J.P., John, D.A., Brooks, E.R., Cassel, E.J., Garside, L.J., Davis, D.A., and Castor, S.B., 2012, Eocene–Early Miocene paleotopography of the Sierra Nevada–Great Basin–Nevadaplano based on widespread ash-flow tuffs and paleovalleys: Geosphere, v. 8, p. 1–27, https://doi.org/10.1130/GES00727.1.

Hoxey, A., Lee, J., and Calvert, A., 2020, Geologic map of the Petrified Spring fault, Gabbs Valley Range, Mineral County, Nevada: Nevada Bureau of Mines and Geology Open-File Report 20-1, scale 1:24,000, 14 p.

Humphreys, E.D., 1995, Post-Laramide removal of the Farallon slab, western United States: Geology, v. 23, p. 987–990, https://doi.org/10.1130/0091-7613(1995)023<0987:PLROTF>2.3.CO;2.

Humphreys, E.D., 2009, Relation of flat slab subduction to magmatism and deformation in the western United States, *in* Kay, S.M., Ramos, V.A., and Dickinson, W.R., eds., Backbone of the Americas: Shallow Subduction, Plateau Uplift, and Ridge and Terrane Collision: Geological Society of America Memoir 204, p. 85–98, https://doi.org/10.1130/2009.1204(04).

Humphreys, E.D., and Coblentz, D.D., 2007, North American dynamics and western U.S. tectonics: Reviews of Geophysics, v. 45, RG3001, https://doi.org/10.1029/2005RG000181.

John, D.A., Thomason, R.E., and McKee, E.H., 1989, Geology and K-Ar geochronology of the Paradise Peak Mine and the relationship of pre–Basin and Range extension to early Miocene precious metal mineralization in west-central Nevada: Economic Geology and the Bulletin of the Society of Economic Geologists, v. 84, p. 631–649, https://doi.org/10.2113/gsecongeo.84.3.631.

Jolivette, P.L., 1993, Least-squares fits when there are errors in X: Computers in Physics, v. 7, p. 208–211, https://doi.org/10.1063/1.168460.

Jones, C.H., 1987, Is extension in Death Valley accommodated by thinning of the mantle lithosphere beneath the Sierra Nevada, California?: Tectonics, v. 6, p. 449–473, https://doi.org/10.1029/TC006i004p00449.

Jones, C.H., Farmer, G.L., and Unruh, J.R., 2004, Tectonics of Pliocene removal of lithosphere of the Sierra Nevada, California: Geological Society of America Bulletin, v. 116, p. 1408–1422, https://doi.org/10.1130/B25397.1.

Kuiper, K.F., Deino, A., Hilgen, F.J., Krijgsman, W., Renne, P.R., and Wijbrans, J.R., 2008, Synchronizing rock clocks of Earth history: Science, v. 320, p. 500–504, https://doi.org/10.1126/science.1154339.

Langille, J., Lee, J., Blisniuk, K., Sharp, W.D., Gosse, J., and Torres, A., 2016, Rates of Quaternary dextral slip within the central Walker Lane, western Nevada: Geological Society of America Abstracts with Programs, v. 48, p. 265–3, https://doi.org/10.1130/abs/2016AM-284345.

Langille, J., Blisniuk, K., Sharp, W.D., and Lee, J., 2018, Rates of Quaternary dextral slip on the Benton Springs fault, central Walker Lane, western Nevada, constrained through U-series dating of offset alluvial fans: Geological Society of America Abstracts with Programs, v. 50, https://doi.org/10.1130/abs/2018RM-313682.

Lechler, A.R., Niemi, N.A., Hren, M.T., and Lohmann, K.C., 2013, Paleoelevation estimates for the northern and central proto–Basin and Range from carbonate clumped isotope thermometry: Tectonics, v. 32, p. 295–316, https://doi.org/10.1002/tect.20016.

Lee, J., Stockli, D.F., Owen, L.A., Finkel, R.C., and Kislitsyn, R., 2009, Exhumation of the Inyo Mountains, California: Implications for the timing of extension along the western boundary of the Basin and Range Province and distribution of dextral fault slip rates across the eastern California shear zone: Tectonics, v. 28, TC1001, https://doi.org/10.1029/2008TC002295.

Lee, J., Blythe, A., and Stockli, D., 2020, Miocene slip along the southern Sierra Nevada range front normal fault: Preliminary low-temperature thermochronology results: Geological Society of America Abstracts with Programs, v. 52, no. 4, paper 2-6, https://doi.org/10.1130/abs/2020CD-347078.

Lifton, Z.M., Newman, A.V., Frankel, K.L., Johnson, C.W., and Dixon, T.H., 2013, Insights into distributed plate rates across the Walker Lane from GPS geodesy: Geophysical Research Letters, v. 40, p. 4620–4624, https://doi.org/10.1002/grl.50804.

Lifton, Z.M., Lee, J., Newman, A.V., and Schroeder, J.M., 2020, Quaternary slip rates on the White Mountains fault zone, eastern California: Implications for comparing geologic to geodetic slip rates across the Walker Lane: Geological Society of America Bulletin, v. 123, https//doi.org/10.1130/B35332.1.

MacNamee, A.F., 2015, Thermochronometric investigation of structural evolution and geothermal systems in extensional settings, Dixie Valley, Nevada [M.S. thesis]: Austin, Texas, University of Texas, 166 p.

McCosby, J.B., 2019, Characterizing the deformation history of the southern Mina Deflection: Field and structural studies in the Huntoon Mountains, California-Nevada [M.S. thesis]: Ellensburg, Washington, Central Washington University, 65 p.

McIntyre, J.L., 1990, Late Cenozoic structure of the central Wassuk Range, Mineral County, Nevada [M.S. thesis]: Corvallis, Oregon State University, 107 p.

McQuarrie, N., and Oskin, M., 2010, Palinspastic restoration of NAVDat and implications for the origin of magmatism in southwestern North America: Journal of Geophysical Research, v. 115, B10401, https://doi.org/10.1029/2009JB006435.

Miller, E.L., Dumitru, T.A., Brown, R.W., and Gans, P.B., 1999, Rapid Miocene slip on the Snake Range-Deep Creek range fault system, east-central Nevada: Geological Society of America Bulletin, v. 111, p. 886–905, https://doi.org/10.1130/0016-7606(1999)111<0886:RMSOTS>2.3.CO;2.

Nagorsen-Rinke, S., Lee, J., and Calvert, A., 2013, Pliocene sinistral slip across the Adobe Hills, eastern California-western Nevada: Kinematics of fault slip transfer across the Mina deflection: Geosphere, v. 9, p. 37–53, https://doi.org/10.1130/GES00825.1.

Nielsen, R.L., 1965, Right-lateral strike-slip faulting in the Walker Lane, west-central Nevada: Geological Society of America Bulletin, v. 76, p. 1301–1308, https://doi.org/10.1130/0016-7606(1965)76[1301:RSFITW]2.0.CO;2.

Oldow, J.S., 1992, Late Cenozoic displacement partitioning in the northwestern Great Basin, *in* Craig, S.D., ed., Structure, Tectonics, and Mineralization of the Walker Lane: Reno, Nevada, Walker Lane Symposium Proceedings, Geological Society of Nevada, p. 17–52.

Oldow, J.S., and Dockery, H.A., 1993, Geologic map of the Bettles Well Quadrangle, Nevada Bureau of Mines and Geology Field Studies Map 1, scale 1:24,000.

Oldow, J.S., and Meinwald, J.N., 1992, Geologic map of the Mina Quadrangle, Nevada Bureau of Mines and Geology Field Studies Map 6, scale 1:24,000.

Parsons, T., Thompson, G.A., and Sleep, N.H., 1994, Mantle plume influence on the Neogene uplift and extension of the U.S. western Cordillera?: Geology, v. 22, p. 83–86, https://doi.org/10.1130/0091-7613(1994)022<0083:MPIOTN>2.3.CO;2.

Petronis, M.S., Zebrowski, P.J., Shields, S.F., Pluhar, C.J., and Lindeman, J.R., 2019, Vertical axis rotation across the eastern Mono Basin and west-central Walker Lane revealed by paleomagnetic data from the Jack Spring tuff: Geochemistry, Geophysics, Geosystems, v. 20, p. 1854–1888, https://doi.org/10.1029/2018GC007682.

Downloaded from http://pubs.geoscienceworld.org/gsa/geosphere/article-pdf/16/5/1249/5148564/1249.pdf
by University of Nevada Reno user

Proffett, J.M., Jr., and Proffett, B.H., 1976, Stratigraphy of the Tertiary ash-flow tuffs in the Yerington District, Nevada: Nevada Bureau of Mines and Geology, Report 27, 28 p.

Reheis, M.C., and Sawyer, T.L., 1997, Late Cenozoic history and slip rates of the Fish Lake Valley, Emigrant Peak, and Deep Springs fault zones, Nevada and California: Geological Society of America Bulletin, v. 109, p. 280–299, https://doi.org/10.1130/0016-7606(1997)109<0280:LCHASR>2.3.CO;2.

Saleeby, J., Le Pourhiet, L., Saleeby, Z., and Gurnis, M., 2012, Epeirogenic transients related to mantle lithosphere removal in the southern Sierra Nevada region, California, part I: Implications of thermomechanical modeling: Geosphere, v. 8, p. 1286–1309, https://doi.org/10.1130/GES00746.1.

Saltus, R.W., and Thompson, G.A., 1995, Why is it downhill from Tonopah to Las Vegas?: A case for a mantle plume support of the high northern Basin and Range: Tectonics, v. 14, p. 1235–1244, https://doi.org/10.1029/95TC02288.

Schmandt, B., and Humphreys, E.D., 2011, Seismically imaged relict slab from the 55 Ma Siletzia accretion to the northwest United States: Geology, v. 39, p. 175–178, https://doi.org/10.1130/G31558.1.

Shaver, S.A., and McWilliams, M., 1987, Cenozoic extension and tilting recorded in Upper Cretaceous and Tertiary rocks at the Hall molybdenum deposit, northern San Antonio Mountains, Nevada: Geological Society of America Bulletin, v. 99, p. 341–353, https://doi.org/10.1130/0016-7606(1987)99<341:CEATRI>2.0.CO;2.

Sonder, L.J., and Jones, C.H., 1999, Western United States extension: How the West was widened: Annual Review of Earth and Planetary Sciences, v. 27, p. 417–462, https://doi.org/10.1146/annurev.earth.27.1.417.

Stewart, J.H., 1988, Tectonics of the Walker Lane belt, western Great Basin: Mesozoic and Cenozoic deformation in a zone of shear, *in* Ernst, W.G., ed., Metamorphism and Crustal Evolution of the Western United States: Englewood Cliffs, New Jersey, Prentice Hall, p. 681–713.

Stewart, J.H., Johannesen, D.C., and Dohrenwend, J.C., 1981, Geologic map of the Hawthorne Quadrangle, Mineral County, Nevada: U.S. Geological Survey, Miscellaneous Field Studies, Map MF-1277.

Stock, G.M., Anderson, R.S., and Finkel, R.C., 2004, Pace of landscape evolution in the Sierra Nevada, California, revealed by cosmogenic dating of cave sediments: Geology, v. 32, p. 193–196, https://doi.org/10.1130/G20197.1.

Stock, G.M., Anderson, R.S., and Finkel, R.C., 2005, Rates of erosion and topographic evolution of the Sierra Nevada, California, inferred from cosmogenic ^{26}Al and ^{10}Be concentrations: Earth Surface Processes and Landforms, v. 30, p. 985–1006, https://doi.org/10.1002/esp.1258.

Stockli, D.F., 1999, Regional timing and spatial distribution of Miocene extension in the northern Basin and Range Province [Ph.D. thesis]: Stanford, California, Stanford University, 239 p.

Stockli, D.F., Surpless, B.E., Dumitru, T.A., and Farley, K.A., 2002, Thermochronological constraints on the timing and magnitude of Miocene and Pliocene extension in the central Wassuk Range, western Nevada: Tectonics, v. 21, p. 10–19, https://doi.org/10.1029/2001TC001295.

Stockli, D.F., Dumitru, T.A., McWilliams, M.O., and Farley, K.A., 2003, Cenozoic tectonic evolution of the White Mountains, California and Nevada: Geological Society of America Bulletin, v. 115, p. 788–816, https://doi.org/10.1130/0016-7606(2003)115<0788:CTEOTW>2.0.CO;2.

Surpless, B., Stockli, D.F., Dumitru, T.A., and Miller, E.L., 2002, Two-phase westward encroachment of Basin and Range extension into the northern Sierra Nevada: Tectonics, v. 21, p. 1002–1014, https://doi.org/10.1029/2000TC001257.

Thatcher, W., Foulger, G.R., Julian, B.R., Svarc, J.L., Quilty, E., and Bawden, G.W., 1999, Present-day deformation across the Basin and Range province, western United States: Science, v. 283, p. 1714–1718, https://doi.org/10.1126/science.283.5408.1714.

Tincher, C.R., and Stockli, D.F., 2009, Cenozoic volcanism and tectonics in the Queen Valley area, Esmeralda County, western Nevada, *in* Oldow, J.S., and Cashman, P.H., eds., Late Cenozoic Structure and Evolution of the Great Basin–Sierra Nevada Transition: Geological Society of America Special Paper 447, https://doi.org/10.1130/2009.2447(13).

Wakabayashi, J., and Sawyer, T.L., 2001, Stream incision, tectonics, uplift and evolution of topography of the Sierra Nevada, California: The Journal of Geology, v. 109, p. 539–562, https://doi.org/10.1086/321962.

Wesnousky, S.G., 2005, Active faulting in the Walker Lane: Tectonics, v. 24, p. 1–35, https://doi.org/10.1029/2004TC001645.

Wright, H.M.N., Lesti, C., Cas, R.A.F., Porreca, M., Viramonte, J.G., Folkes, C.B., and Giordano, G., 2011, Columnar jointing in vapor-phase-altered, non-welded Cerro Galán Ignimbrite, Paycuqui, Argentina: Bulletin of Volcanology, v. 73, p. 1567–1582, https://doi.org/10.1007/s00445-011-0524-6.

Downloaded from http://pubs.geoscienceworld.org/gsa/geosphere/article-pdf/16/5/1249/5148564/1249.pdf
by University of Nevada Reno user